Advanced Drug Delivery Reviews 154–155 (2020) 123–141

Contents lists available at ScienceDirect

Advanced Drug Delivery Reviews

journal homepage: www.elsevier.com/locate/addr

Nuclear imaging approaches facilitating nanomedicine translation

Carlos Pérez-Medina [a,b,*], Abraham J.P. Teunissen [b], Ewelina Kluza [c], Willem J.M. Mulder [b,c,d], Roy van der Meel [c,*]

[a] Centro Nacional de Investigaciones Cardiovasculares (CNIC), Madrid, Spain
[b] BioMedical Engineering and Imaging Institute, Icahn School of Medicine at Mount Sinai, NY, New York, United States of America
[c] Laboratory of Chemical Biology, Department of Biomedical Engineering and Institute for Complex Molecular Systems, Eindhoven University of Technology, Eindhoven, the Netherlands
[d] Department of Oncological Sciences, Icahn School of Medicine at Mount Sinai, New York, NY, USA

ARTICLE INFO

Article history:
Received 1 June 2020
Received in revised form 8 July 2020
Accepted 17 July 2020
Available online 25 July 2020

Keywords:
Quantitative imaging
Nanomedicine
Radiolabeling
Clinical translation
Positron emission tomography
Single-photon emission computed tomography

ABSTRACT

Nanomedicine approaches can effectively modulate the biodistribution and bioavailability of therapeutic agents, improving their therapeutic index. However, despite the ever-increasing amount of literature reporting on preclinical nanomedicine, the number of nanotherapeutics receiving FDA approval remains relatively low. Several barriers exist that hamper the effective preclinical evaluation and clinical translation of nanotherapeutics. Key barriers include insufficient understanding of nanomedicines' *in vivo* behavior, inadequate translation from murine models to larger animals, and a lack of patient stratification strategies. Integrating quantitative non-invasive imaging techniques in nanomedicine development offers attractive possibilities to address these issues. Among the available imaging techniques, nuclear imaging by positron emission tomography (PET) and single-photon emission computed tomography (SPECT) are highly attractive in this context owing to their quantitative nature and uncontested sensitivity. In basic and translational research, nuclear imaging techniques can provide critical quantitative information about pharmacokinetic parameters, biodistribution profiles or target site accumulation of nanocarriers and their associated payload. During clinical evaluation, nuclear imaging can be used to select patients amenable to nanomedicine treatment. Here, we review how nuclear imaging-based approaches are increasingly being integrated into nanomedicine development and discuss future developments that will accelerate their clinical translation.

Contents

* Corresponding authors.
E-mail addresses: cperez@cnic.es (C. Pérez-Medina), r.v.d.meel@tue.nl (R. van der Meel).

https://doi.org/10.1016/j.addr.2020.07.017

1. Introduction

Nanomedicine offers attractive options to improve the treatment of conditions such as cancer, atherosclerosis, autoimmune disorders and infectious diseases [1,2]. Nanomedicines are generally designed to improve a drug's bioavailability by altering its pharmacokinetics and biodistribution. As a result, the therapeutic index of a drug can be improved due to enhanced efficacy reduced toxicity, or both. For example, Vyxeos® (liposomal daunorubicin plus cytarabine) was approved by the US Food and Drug Administration (FDA) in 2017 for treating acute myeloid leukemia after demonstrating improved overall survival compared to standard of care [3,4]. More recently, nanocarrier technology has also enabled the clinical translation of RNA therapeutics, which need protection from nucleases in the circulation and generally require intracellular delivery [5]. Onpattro®, the first ever small interfering RNA (siRNA) therapeutic, was approved in 2018 for treating transthyretin-related hereditary amyloidosis [6,7]. Excitingly, owing to the inherent interactions between nanomaterials and immune cells, many efforts are currently geared towards developing nanomedicine-based immunotherapies [8–12].

Despite these developments and the vast number of preclinical studies reporting on nanomedicine development, the number of nanotherapeutics that reach the clinic is relatively low. Several factors contribute to this discrepancy. First, nanomedicine development has traditionally focused on oncology and the vast majority of nanomedicines approved by the FDA or under evaluation are intended for treatment of solid tumors [13]. Following the report on the *enhanced permeability and retention* (EPR) effect that describes how macromolecules accumulate in solid tumors [14,15], this phenomenon was quickly embraced as an all-encompassing guiding principle for nanomedicine design. Although this culminated in the approval of the first nanomedicine in 1995, called Doxil® (liposomal doxorubicin), for treatment of Kaposi's sarcoma [16], it is clear now that there is a high inter- and intra-patient variability of the EPR effect in humans. In addition, a large meta-analysis of preclinical studies indicated limited uptake of cancer nanomedicines in solid tumors [17], while a recent fundamental study from the same group demonstrated that nanoparticle uptake in tumors is mechanistically different than previously thought [18]. Second, 'novel' nanomedicine formulations reported in literature often have low translational potential due to poor *in vivo* stability as well as issues related to scalability and cost-effectiveness [19]. Finally, regardless of the therapeutic indication, the most important translational hurdle is the lack of understanding nanomedicines' *in vivo* behavior. As a result, in preclinical nanomedicine an excessive reliance on mouse models exists, while in a clinical setting, efficient patient stratification strategies are nonexistent [20].

Bridging the gap between benchtop and bedside nanomedicine requires reliable solutions to better characterize nanotherapeutics' *in vivo* behavior. Non-invasive imaging represents a powerful tool that allows visualizing nanomaterials' fate *in vivo*, providing objective readouts that enable efficient decision making, *e.g.*, regarding patient stratification [21]. Most available imaging techniques, including magnetic resonance imaging (MRI), optical imaging methods as well as nuclear imaging by positron emission tomography (PET) and single-photon emission computed tomography (SPECT), have been used to study nanoparticles' *in vivo* behavior. However, not all imaging techniques are equally suited for the quantitative assessment of a nanotherapeutic's performance *in vivo*.

In this review, we will discuss how non-invasive imaging using PET and SPECT can be used to determine nanoparticles' pharmacokinetic properties, biodistribution and therapeutic effects in a truly quantitative manner [22–24]. To that end, we first provide an overview of the imaging techniques that are commonly used to study nanomedicines *in vivo*, focusing on their ability to yield quantitative information. Second, we highlight the most promising nanomedicine radiolabeling methods. We then discuss how quantitative nuclear imaging is used to preclinically evaluate nanotherapeutics and to facilitate their clinical translation. Finally, we provide a perspective on future developments in the field, including further advancement in hybrid imaging techniques, high-throughput screening and data analyses using machine learning and artificial intelligence.

2. Imaging techniques in nanomedicine research

Imaging allows studying nanomaterials' *in vivo* behavior in a minimally- or non-invasive manner. As such, it has revolutionized preclinical (nanomedicine) research and, combined with big data analysis, it will facilitate imaging-guided personalized medicine [25,26]. MRI and X-ray computed tomography (CT) excel at providing anatomical information, but exhibit poor sensitivity for visualizing exogenously administered contrast agents. On the other hand, optical and nuclear imaging techniques are hot-spot techniques that require the administration of labeled species to generate the detected signal. Nanomaterials containing these contrast- or signal-generating agents can therefore be traced *in vivo* by the corresponding imaging technique. Each technique available for imaging nanomedicines *in vivo* is characterized by differences in cost, spatiotemporal resolution, and sensitivity. Although a detailed description of all different imaging techniques used for nanomedicine evaluation is beyond the scope of this review, we have summarized their key features in Table 1. In this section, we briefly feature the most widely used techniques in nanomedicine research and development, focusing on their ability to generate quantitative imaging data.

CT and MRI are both very powerful anatomical imaging techniques, albeit for different reasons. CT derives images from the interaction of X-ray photons with matter. Although CT uses ionizing radiation to generate images, it is fast, relatively cheap and easy to operate. Quantitative information can be directly derived from CT images. However, its use for imaging nanomedicines is hampered by its very low contrast sensitivity, which requires the administration of large amounts of exogenous agents. This is why only a small number of studies have used CT contrast agents to track nanoparticles *in vivo* [27]. MRI, on the other hand, is an ionizing radiation-free imaging technique that generates images based on a certain nuclide's spin relaxation (most typically ^{1}H) when subjected to an external magnetic field. ^{1}H-MRI generates anatomical images that are characterized by excellent soft-tissue contrast. MR imaging has been employed to track nanomaterials *in vivo* by functionalizing them with paramagnetic (manganese, gadolinium) or superparamagnetic (iron oxide) contrast agents. Contrast quantification can be derived from images acquired pre- and post-administration of the functionalized nanomaterial. However, this quantification is not straightforward, as the generated contrast not only depends on the agent's concentration but also is affected by other factors, such as relaxivity, tissue properties and magnetic field inhomogeneities. In addition, contrast quantification methods are sequence-dependent, require standardization and frequently suffer from non-linearity at either end of the calibration curve. Moreover, the limited contrast sensitivity (μM to mM) and toxicity concerns severely limit the clinical use of some of these agents. For these reasons, contrast-based MR imaging cannot provide truly quantitative insight on nanoparticle tissue

Table 1
Key features of imaging techniques commonly used for nanomedicine development including examples of imaging agents [40].

Technique	Physical phenomenon	Spatial resolution	Imaging agent	Sensitivity	Penetration in tissue	Cost	Scan time
MRI [41]	Nuclear spin relaxation	<0.1 mm (P) 1–2 mm (C)	Gd, Mn, iron oxide	μM-mM	No limit	$$	min/h
Optical [42,43]	Visible/IR photon emission	1–5 mm (*in vivo*)	fluorophores	nM	mm-cm	$	min
CT [44]	X-ray absorption/deflection	<0.2 mm (P) 0.5–1 mm (C)	Iodine, Au	mM	No limit	$	min
PET [41,45]	β^+ annihilation-derived γ photon emission	1–2 mm (P) 6–10 mm (C)	^{18}F, ^{64}Cu, ^{68}Ga, ^{89}Zr	fM	No limit	$$$	min
SPECT [41,45]	X-ray and γ photon emission	0.5–2 mm (P) 7–15 mm (C)	^{99m}Tc, ^{111}In ^{123}I, ^{125}I	<pM	No limit	$$	min

IR = infrared; (P) = preclinical; (C) = clinical.

accumulation. Alternatively, MRI can be used in a "hot-spot" imaging fashion to investigate nanomaterials' *in vivo* behavior. This approach relies on the use of compounds containing MR-active nuclei of very low natural abundance in the body, such as ^{19}F [28]. Nanoparticles can be loaded with these ^{19}F-based compounds and tracked *in vivo*. While recent studies have demonstrated the feasibility of this approach [29,30], ^{19}F-MRI has intrinsic sensitivity limitations that require the administration of high doses of the ^{19}F-based compounds, which imposes high tracer load per nanoparticle and could be toxic in humans.

Similarly, optical molecular imaging techniques, such as near-infrared fluorescence (NIRF) imaging or fluorescence molecular tomography (FMT), can provide valuable information on a nanomaterial's *in vivo* behavior, especially because it offers the possibility for multiplexing, *i.e.* the simultaneous acquisition of multiple signals. This can be achieved by using multiple fluorophores, which are detected in different emission channels, and the obtained information is subsequently de-multiplexed. Optical imaging also allows the evaluation of nanoparticle dynamics by Förster's resonance energy transfer (FRET) [31], which can be used to study nanoparticle formation [32] or *in vivo* stability [33]. Moreover, intravital microscopy enables visualization of nanoparticle accumulation at the cellular level. The limitations associated with these techniques result from the emitted light's limited tissue penetration, fluorophore bleaching and quenching, or tissue absorption, which make them semi-quantitative at best. In 2D (planar) techniques, such as fluorescence reflectance imaging, the signal is surface-weighted so that fluorophores close to the surface appear brighter than those deeper inside the tissue. Collectively, these issues make absolute quantification challenging when using optical imaging methods.

Nuclear imaging techniques rely on the detection of gamma photons emitted by exogenously administered radioactive substances, generally called radiotracers. Specifically, PET scanners detect coincidence events, *i.e.* the two 511 keV photons emitted in opposite directions after positron-electron annihilation, whereas SPECT images derive from X-ray and gamma photons associated with nuclear state transitions. SPECT scanners use collimators to restrict photon incidence angle, which results in a lower counting efficiency and sensitivity compared to PET. Although both techniques have no practical tissue penetration limit, certain attenuation of the signal occurs due to loss of photon detection because of their absorption by the body or their scattering out of the detector's field of view. Nevertheless, both PET and SPECT are extremely sensitive, as they allow the detection of sub-pM tracer concentrations. Given the low amounts of imaging agent needed, the biological processes under study are therefore undisturbed. Similar to PET imaging, the latest advances in detector technology and data post-processing have made truly quantitative SPECT imaging possible [34]. On the downside, both techniques suffer from spatial resolution limitations and a dearth of anatomical reference information. For this reason, PET and SPECT scanners are typically combined with CT and lately also MRI in hybrid imaging scanners. The co-registered CT information can thus be used not only to provide anatomical reference, but also to generate attenuation correction maps that are critical for accurate quantification purposes. These maps can also be generated from MRI-derived anatomical information albeit through different transformation approaches since the MRI signal does not directly correlate to tissue density. For truly quantitative nuclear imaging by PET and SPECT, images have to be corrected for several issues, most prominently the already mentioned photon attenuation, but also scattering, dead time, radionuclide decay and branching ratio. Additionally, emitted photon energy has to be considered for SPECT imaging, since too low energy photons will not efficiently leave the body, whereas too high energy photons will penetrate through the collimator resulting in signal contamination.

As a result of the high sensitivity of nuclear imaging techniques only a small amount of radionuclide is required, thereby minimizing modification of the nanotherapeutic platform. However, radiolabeled nanoparticle formulations may still behave differently compared to their unmodified variants and thus need to be extensively characterized. Another exciting feature of SPECT is its ability to discriminate between different isotopes based on their emitted photon energy, which allows quantitative tracking of multiple isotope-labeled nanomaterials [35]. This can be exploited to derive information on formulation stability and dynamics [36,37] – by labeling the carrier and the payload with different isotopes– which can have a critical impact on *in vivo* performance. Multi-isotope PET imaging is also feasible, even with standard scanners that cannot distinguish between radionuclides based on coincidence event detection. Discrimination in this case relies on differences in half-lives and kinetic assumptions, which yield suboptimal results. Recent developments, however, have prompted real multiple isotope detection based on concomitant gamma photons that accompany radioactive decay by positron emission [38,39]. Taken together, these features place nuclear imaging techniques at the forefront of quantitative *in vivo* assessment of nanomedicines' performance and translational development.

3. Strategies for radiolabeling nanomedicines

Employing nuclear imaging to investigate nanotherapeutics *in vivo* requires matching radionuclides, nanocarriers, and radiolabeling strategies. Naturally, the radionuclide also needs to be compatible with the detection method used, with SPECT and PET requiring gamma- and positron-emitting radionuclides, respectively. Furthermore, efficient nuclear imaging requires radionuclides with high specific activity (*i.e.* the number of decay events per second per quantity of material) and branching ratio (*i.e.* the fraction of these events that proceed through the decay mode required for imaging). Given these criteria, it is no surprise that of the approximately 1800 radionuclides known only a limited number are routinely used to radiolabel nanotherapeutics and nanotracers (Table 2). From this overview it also becomes apparent that only radionuclides with short physical half-lives (roughly 1 h to 1 month) are routinely used. This selection window likely results from a need to have sufficient time for radiolabeling and monitoring of the biological processes under scrutiny, while simultaneously minimizing the patient's exposure to radioactivity.

Besides radionuclides' physical properties and their suitability for nuclear imaging, the radioisotopes' compatibility with the desired

Table 2
Properties and applications of radionuclides commonly used for labeling nanotherapeutics and nanotracers.

Radionuclide (half-life)	Decay mode (branching ratio)	Imaging modality	Commonly labeled nanocarrier materials	Typical radiolabeling strategies
^{18}F (100 min)	β^+ (97%)	PET	Protein [53], carbon [54], metal [55], polymer [56,57], nanocrystal [58,59]	Hot-plus-cold Surface functionalization
^{64}Cu (12.7 h)	β^+ (18%)	PET	Metal [60–62], lipid [63,64], DNA [65], polymer [66,67], glucan [68], silica [69], peptide [70,71], nanocrystal [72,73]	Hot-plus-cold Physical entrapment Ion exchange Surface functionalization Chelation
^{68}Ga (68 min)	β^+ (89%)	PET	Metal [74], nanocrystal [75,76], polymer [77]	Hot-plus-cold Surface functionalization Chelation
^{69}Ge (39.1 h)	β^+ (100%)	PET	SPION [78,79]	Surface functionalization
^{89}Zr (3.27 d)	β^+ (23%)	PET	Lipid [80–82], nanocrystal [83,84], glucan [85], silica [86,87], polymer [88], carbon [89]	Surface functionalization Chelation
^{99m}Tc (6.03 h)	IT (100%)	SPECT	Carbon [90], lipid [91], glucan [92], DNA [93], protein [94], metal [91]	Physical entrapment Surface functionalization Chelation
^{111}In (67.3 h)	EC (100%)	SPECT	lipid, polymer, peptide, metal [95–99], carbon [100]	Hot-plus-cold Surface functionalization Chelation
^{124}I (4.18 d)	β^+ (23%)	PET	Metal [101], polymer [102], lipid [103], silica [104]	Physical entrapment Surface functionalization
^{125}I (59.4 d)	EC (100%)	SPECT	Nanocrystal [105], metal [106,107]	Physical entrapment Surface functionalization Chelation
^{131}I (8.02 d)	β^- (100%)	SPECT	Protein [108], polymers [109,110], carbon [111], metal [112]	Hot-plus-cold Ion exchange Surface functionalization
^{153}Sm (46.3 h)	β^- (100%)	SPECT	Nanocrystal [113–115]	Hot-plus-cold
^{177}Lu (6.73 d)	β^- (100%)	SPECT	Metal [116–118], polymer [119]	Surface functionalization Chelation
^{186}Re (3.72 d)	β^- (93.1%)	SPECT	Liposomes [120–122]	Physical entrapment
^{188}Re (17.0 h)	β^- (100%)	SPECT	Liposomes [123–125]	Physical entrapment
^{198}Au (27.0 d)	β^- (100%)	SPECT	Metal [35,126–128]	Hot-plus-cold Particle beam transmutation
^{225}Ac (10.0 d)	α (100%)	SPECT	Lipid [129,130], polymers [131,132], carbon [89], nanocrystal [133]	Hot-plus-cold Physical entrapment Chelation

IT = isomeric transition, EC = electron capture, SPION = superparamagnetic iron oxide nanoparticle. The references mentioned serve as examples and are by no means exhaustive.

nanocarrier and radiolabeling strategy is also important; with cost, scalability, radiochemical yield and purity, and the reaction's duration key factors to consider. Generally, procedures where the radionuclides are introduced post nanoparticle formulation are desirable, since alternative methods (*e.g.*, hot-plus-cold precursors or physical entrapment, see below) potentially expose the worker to radiation throughout the entire formulation process. Lastly, nanocarriers' retention of recoiling daughter radionuclides is desirable and especially relevant to the relatively heavy α-emitters used for radionanotherapy (*e.g.*, ^{213}Bi consecutively decays into radioactive ^{213}Po and ^{209}Pb which are not necessarily all retained to the same degree) [46]. The many variations on nanoparticle radiolabeling strategies have been extensively reviewed elsewhere [24,47–52]. Rather, we will here provide an overview of the six main approaches used and discuss their scope and limitations based on representative examples (Fig. 1).

3.1. Hot-plus-cold precursors

In this approach a radioactive analogue of one or more of the nanotherapeutic's constituents (*e.g.*, the drug) is created, for example by chelating the radionuclide [134,135] or by functionalizing it with radioactive ^{18}F [56,136]. Subsequently, these building blocks are used to formulate a radioactive version of the nanocarrier. A very similar procedure relies on doping metal-based nanocarriers by mixing the bulk metal with a small amount of the radionuclide [137,138]. Creating nanocarriers using radioactive precursors minimizes altering the nanoparticles' properties and generally leads to stable formulations. However, it requires the precursors to withstand the sometimes harsh conditions associated with nanocarrier formulation and can pose health risks by exposing the worker to radiation during the entire formulation process. Related, it is often necessary to start with high amounts of radioactivity, which is needed to compensate for decay during both the functionalization and formulation process.

3.2. Physical entrapment

Rather than functionalizing the nanocarriers' constituents, it is also possible to physically entrap radionuclides. An example is the surface labeling of liposomes in which the radionuclide is trapped inside the lipid bilayer without the use of dedicated chelators [24,139]. Such formulations are often unstable *in vivo* as lipid-radionuclide interactions are generally weak and the bilayer too fluid to prevent release. In a related and often superior approach, the radionuclide is incorporated inside hollow nanocarriers, such as the interior of liposomes or carbon nanotubes. This can be achieved by encapsulating the radioisotopes during formulation, through passive diffusion from the nanocarriers' exterior to their interior, or with the help of ionophores [24,140]. Physical entrapment of radionuclides is generally a simple methodology that minimizes the risk of altering the nanocarriers' properties. However, it is only applicable to a few nanocarrier types and some variations can be unstable *in vivo*. Furthermore, in cases where the encapsulation process is lengthy (*e.g.*, when the radionuclide is

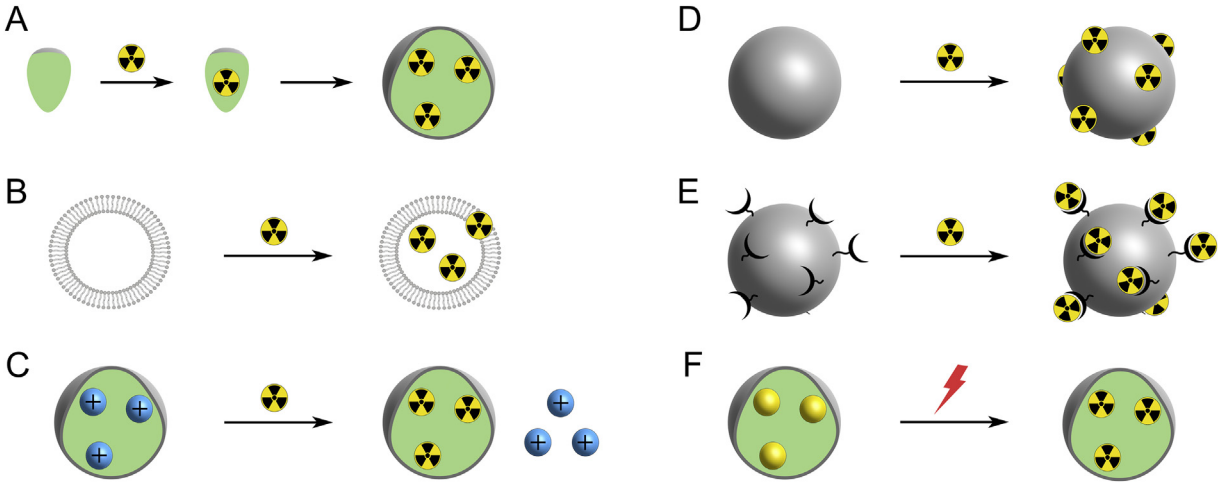

Fig. 1. Schematic overview of the predominant nanocarrier radiolabeling strategies used in nanomedicine and biomedical imaging. **A**) hot-plus-cold precursors, **B**) physical entrapment, **C**) cation exchange, **D**) surface functionalization, **E**) post-formulation chelation, **F**) particle beam transmutation.

incorporated during nanoparticle formulation), this procedure can expose the worker to relatively large amounts of radiation.

3.3. Cation exchange

One way to increase the stability of entrapped radionuclides is by forming ionic bonds. During cation exchange-mediated radiolabeling, part of the cations in a nanocrystal's lattice is substituted with a positively charged radionuclide. Using this approach, Sun et al. replaced Zn in CdSe/ZnS quantum dots with ^{64}Cu and demonstrated these nanocarriers' use as PET and self-illuminating Cerenkov imaging agents [72]. Similarly, $NaLuF_4$:Yb,Gd,Tm nanoparticles have been radiolabeled with ^{153}Sm in quantitative yields, producing SPECT imaging tracers displaying upconversion luminescence [73]. To the best of our knowledge these are the only two examples of this approach reported, which is somewhat surprising as cation exchange using “cold” ions is widely used [141,142]. Explanations for this discrepancy might lie in the availability [143] and physicochemical properties of the required radioisotopes, as well as the relatively limited use of inorganic nanocrystals in nanomedicine. However, the high *in vivo* stabilities and interesting optical properties of nanocrystals make them highly relevant for dual-modality imaging applications, warranting further investigation of this approach [144–147].

3.4. Surface functionalization

Radionuclides can also be bound to a nanoparticle's surface (or porous interior). In its simplest form this is achieved through chemisorption, in which a covalent bond is formed directly between the radionuclide and the unfunctionalized nanoparticle's exterior, for example by coupling ^{125}I to silver nanoparticles [148]. In a slightly more complex approach, nanocarriers' surface can be made reactive towards the bare radionuclide. In this manner, ^{123}I was coupled to gold nanoparticles' functionalized with tannic acid [101]. Alternatively, the radioisotope can be functionalized to allow its coupling to the nanocarrier. Using this methodology, ^{18}F-labeled and thiol-containing compounds have been linked to gold nanoparticles [149], and dextran nanoparticles radiolabeled using azide-alkyne “click” chemistry [150]. Formulations made through these procedures are generally highly stable as the radionuclides are covalently bound. In a less-robust but more widely applicable variation, the radionuclide is bound to a chelator which is subsequently coupled to the nanocarriers' surface; representing a modified version of chelation-based radiolabeling *vide infra* [116,118,151].

3.5. Post-formulation chelation

Nanocarriers' exterior can also be functionalized with chelators to bind radionuclides post-formulation. Due to the relatively large size of most chelators - and their location on the nanocarriers' exterior - this method is relatively prone to altering a nanocarriers' properties and leaves the radionuclide vulnerable to interactions with other compounds [64]. However, the many types of chelators, their ability to chelate a large variety of radionuclides, and the ease with which chelators can be coupled to virtually all types of nanocarriers make this radiolabeling approach one of the most widely used (Table 1). The wide use of chelator-based radiolabeling warrants a more detailed description, which we will provide based on our own experience in radiolabeling lipid nanocarriers with ^{89}Zr, used for PET imaging (Fig. 2). In this procedure, a phospholipid's headgroup is functionalized with a chelator (deferoxamine, DFO) and mixed with bulk lipid at a concentration of 0.5–1.0 wt%. This mixture is subsequently formulated into the desired nanocarrier (*e.g.*, liposomes [80], lipid decorated quantum dots [152] or reconstituted high-density lipoprotein [81,153]). In parallel, ^{89}Y is bombarded with protons to yield ^{89}Zr, which is dissolved in aqueous oxalic acid and later neutralized with Na_2CO_3 to a pH between 6.8 and 7.5. Subsequently, the aqueous nanocarrier suspension is mixed with the ^{89}Zr solution and incubated at 37 °C for approximately 1 h. Afterwards, unbound ^{89}Zr is removed using a desalting column or centrifugal filtration to yield radiolabeled nanocarriers. Before administration, radio-TLC or radio-size-exclusion chromatography is used to determine radiochemical purity, which is typically above >95%. Radiochemical yields are usually well above 90%.

3.6. Particle beam transmutation

Yet another way to radiolabel nanoparticles is through particle beam transmutation [154–158]. In this relatively new but promising approach, nanocarriers are formulated containing stable precursors of the desired radionuclide and subsequently irradiated with neutrons or protons to transmutate these isotopes, *e.g.*, by converting stable ^{165}Ho into radioactive ^{166}Ho [154]. This approach minimizes the presence of unbound radionuclides and thereby eliminates the need for post-radiolabeling purification steps, which could be particularly useful when using short-lived radionuclides [156]. However, most organic compounds are unstable under the required conditions, thereby restricting this method's applicability to inorganic nanocarriers. Furthermore, widespread clinical use of this radiolabeling approach will likely be hindered by the limited availability of particle beams.

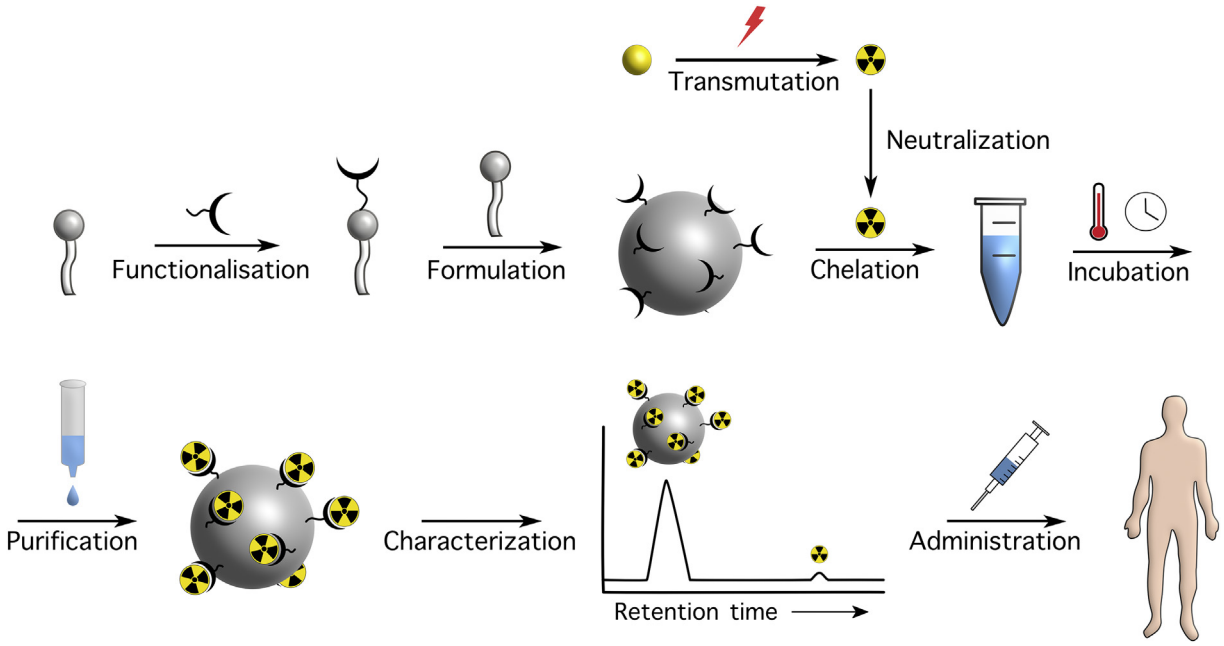

Fig. 2. Schematic of a typical lipid nanoparticle radiolabeling procedure relying on post-formulation chelation of radionuclides. A chelator-functionalized lipid is formulated in the nanocarrier and subsequently mixed with the radionuclide at an optimal pH. After incubation, unbound radionuclide is removed, typically by dialysis, column chromatography, or filtration, and the radiochemical purity of the product assessed using radio-thin-layer chromatography or radio-size-exclusion chromatography.

4. Nuclear imaging in basic nanomedicine research

Preclinically, nuclear imaging techniques can aid in elucidating nanomedicines' *in vivo* behavior in small and large animal models by providing quantitative data on pharmacokinetic parameters, biodistribution, targeting and drug delivery [159] (Fig. 3A). Importantly, these techniques offer the possibility to do this longitudinally in the same subject. The circulation time and tissue accumulation of nanomedicines are, in general, directly related to their therapeutic effect. Therefore, the ability to quantitatively determine nanomedicines' pharmacokinetic parameters and biodistribution is key for efficient development and translation. In this section, we discuss relevant literature on the use of nuclear imaging for early nanomedicine development and optimization. While most studies generalize the labeled nanocarrier's signal to its payload, we also focus on studies that evaluate the cargo's behavior through radiolabeling of the payload itself.

4.1. Biodistribution and pharmacokinetics

The ability to non-invasively derive truly quantitative information using nuclear imaging techniques has been extensively exploited to assess critical nanomedicine *in vivo* performance parameters such as biodistribution and pharmacokinetics. Due to their modularity, stability, ease of production and *in vivo* performance, liposomes are the most widely used nanocarrier platform for drug delivery purposes. Indeed, almost 50% of clinically approved nanomedicines are liposomal formulations [13]. This is also reflected in the number of preclinical studies that report the use of PET and SPECT to characterize or study the behavior of liposomes *in vivo* [24]. We and others have developed liposome radiolabeling strategies that enable *in vivo* visualization of these nanoparticles by PET and SPECT. Using a surface chelation approach with a chelator-modified phospholipid (Fig. 2), we developed a high-yielding ^{89}Zr radiolabeling method for liposomes [160]. This modular approach was used to longitudinally monitor the liposomes' biodistribution and tumor accumulation over a period of 5 days in tumor-bearing mice. Liposomes have also been efficiently labeled with iodine-124 (^{124}I) by remote loading [103] (Fig. 3B). The biodistribution of such radiolabeled liposomes, as assessed by PET imaging, differed significantly from that typically observed for similar long-circulating liposomes, which likely reflects the non-residualizing properties of ^{124}I.

Nanotherapeutic modulation of the immune system, *i.e.* nanoimmunotherapy, has become a promising field within nanomedicine research. Some nanoparticle platforms, such as high-density lipoprotein (HDL), can selectively interact with certain immune cell populations to trigger a specific response [161]. In the last decade, we have pioneered the use of HDL nanobiologics to treat atherosclerosis in several animal models through macrophage-targeted drug delivery [153,162,163]. More recently, we have expanded their use to other disease contexts like organ transplantation [164] and cancer. As an integral part of the nanobiologics' development, we implemented ^{89}Zr labeling approaches to track the different components of the nanoparticle formulation, *i.e.* the protein component (apolipoprotein A1, apoA-I) or the cargo (phospholipids, hydrophobic payload) [165–167].

With the 2018 FDA-approval of Onpattro® (patisiran), an siRNA-containing lipid nanoformulation for treatment of hepatic amyloidosis [6,7], the field of RNA nanotherapeutics (and nanomedicine in general) received a tremendous boost. In this area of nanomedicine research, nuclear imaging has also been used at early stages of development, most typically to assess the biodistribution of radiolabeled RNA loads [168,169]. For example, Bartlett et al. used PET and bioluminescence imaging to quantify the *in vivo* biodistribution and therapeutic activity of cyclodextrin-siRNA nanoparticles [168]. They conjugated DOTA to the 5′ end of siRNA followed by complexation of ^{64}Cu. PET imaging showed that ^{64}Cu-DOTA-siRNA displayed a rapid hepatic and urinary clearance, with biphasic blood clearance kinetics. The biodistribution of the ^{64}Cu-DOTA-siRNA packaged into transferrin-targeted nanoparticles was similar to that of naked ^{64}Cu-DOTA-siRNA with only a slight time delay. Similarly, Hatanaka et al. developed an ^{18}F labeling method for siRNA and evaluated the biodistribution and pharmacokinetics of naked ^{18}F-labeled siRNA *versus* cationic liposome/^{18}F-labeled siRNA complexes using PET imaging [170]. The authors found that the former was rapidly cleared from blood through renal excretion, whereas the latter accumulated predominantly in the lungs.

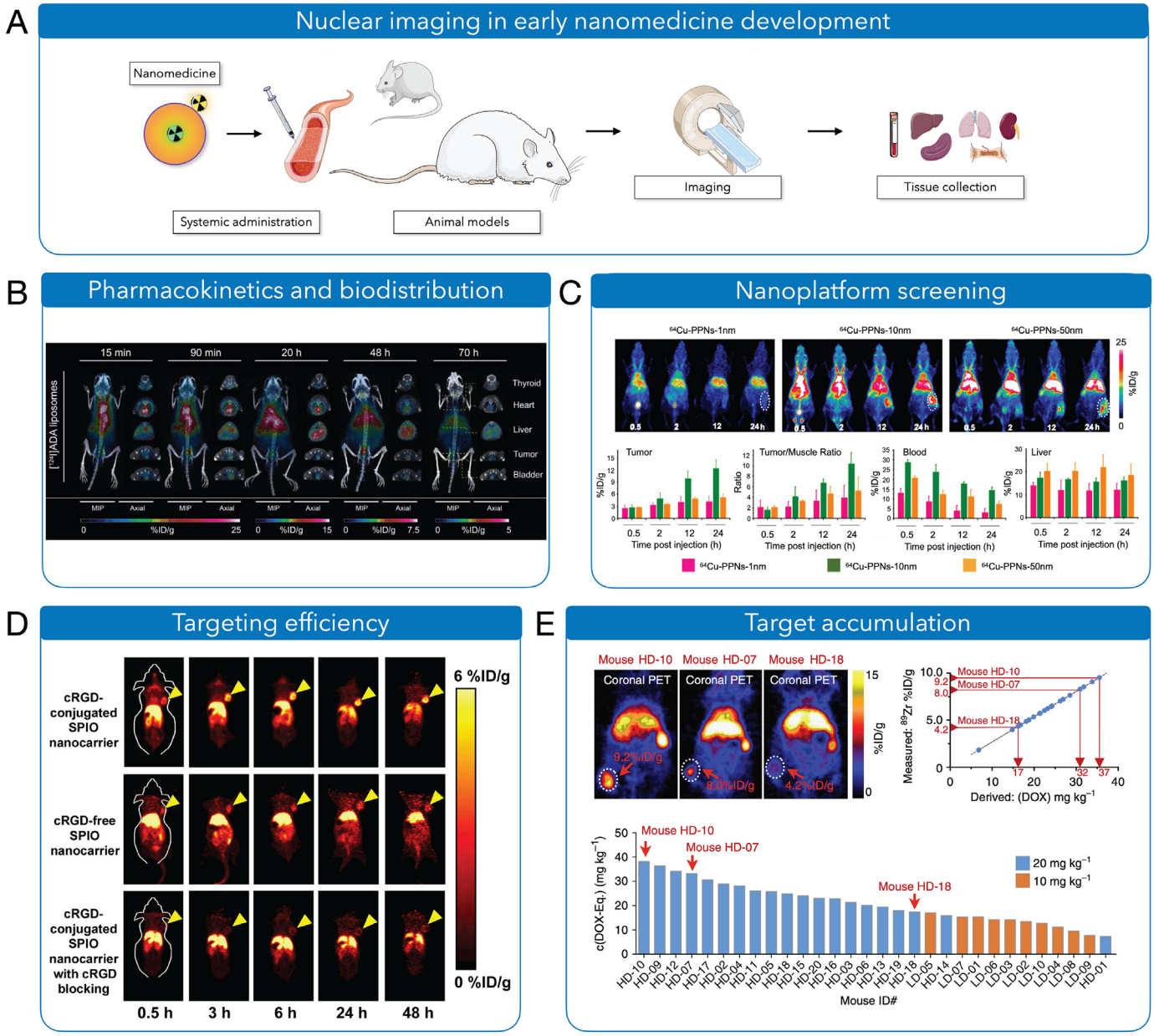

Fig. 3. Nuclear imaging in basic nanomedicine research. **A**) PET and SPECT have been extensively used in early nanomedicine development. The radiolabeled formulation under study is administered to relevant small animal disease models and noninvasively monitored using nuclear imaging to afford quantitative information on its *in vivo* behavior. Importantly, the imaging data thus obtained can be validated by *ex vivo* radioactivity counting and autoradiographic analysis. **B**) The pharmacokinetics and biodistribution of ^{124}I-labeled liposomes were monitored longitudinally over 3 days by PET imaging. Reprinted with permission from Engudar et al. [103]. Copyright 2018 Ivyspring International Publisher. **C**) This kind of *in vivo* data can be integrated in screening procedures to select optimal formulation features. Three pegylated porphyrin nanocomplexes of different sizes were radiolabeled with ^{64}Cu and their biodistribution was monitored longitudinally over 24 h using PET. The quantitative information derived from these imaging experiments revealed that the 10 nm nanoparticle had the best pharmacokinetic profile and highest tumor accumulation and was therefore selected for further evaluation. Reprinted with permission from Yu et al. [119]. Copyright 2018 Wiley-VCH. **D**) The effect of targeting ligands on doxorubicin-loaded iron oxide nanoparticles was studied by PET imaging. Thus, tumor uptake of ^{64}Cu-labeled, cRGD-decorated nanoparticles was higher than for the non-targeted analogs. Reprinted with permission from Yang et al. [174]. Copyright 2011 Elsevier. **E**) A nanotherapeutic's delivered dose in tumors can be determined using a PET nanoreporter approach. Using ^{89}Zr-labeled liposomes as companion imaging for Doxil, we were able to derive the intratumoral doxorubicin delivered dose from the quantified ^{89}Zr PET signal. Pérez-Medina et al. [80]. Copyright 2016 Springer Nature.

Importantly, this type of information can be used in imaging-guided screening studies to identify optimal formulation features. Thus, using the abovementioned ^{89}Zr labeling strategies, we have screened promising candidates in an anti-atherosclerosis nanomedicine library by PET imaging [145]. Following a similar approach, Koziolová et al. used PET imaging of ^{89}Zr-labeled *N*-(2-hydroxypropyl)methacrylamide (HPMA) nanoparticles to study the influence of polymer length and dispersity on their *in vivo* behavior [171]. In three recent studies, imaging-based analyses were implemented to understand the influence of composition and morphology on *in vivo* behavior. In the first one, Indium-111 was used to label polystyrene-*b*-poly(ethylene oxide) micelles of different morphologies and study by SPECT how the morphological differences impacted the micelles' *in vivo* behavior [172]. In the second study, antioxidant cerium oxide nanoparticles were prepared by a co-precipitation method in the presence of zirconium chloride [^{89}Zr]. The radioisotope was physically entrapped in the nanoparticle core, and this enabled PET imaging evaluation of differently coated formulations [173]. Finally, PET imaging was used to screen differently sized porphyrin-PEG

nanocomplexes for optimal tumor accumulation. The nanocomplexes were labeled with ^{64}Cu and their biodistribution was monitored longitudinally over a 24-h period. Based on quantitative PET imaging data, the authors identified a 10-nm nanocomplex as the optimal nanoplatform for therapeutic purposes [119] (Fig. 3C).

4.2. Targeting efficiency

Nuclear imaging has also been used to quantify how much nanomaterial reaches the target tissue. Andresen et al. radiolabeled liposomes with ^{64}Cu by remote loading and used the radioactive nanoparticles to quantify their accumulation in tumors, as well as to investigate their biodistribution and pharmacokinetics, by PET imaging [175]. These liposomes can be used as surrogate imaging companions to quantify tumor accumulation of radiotherapeutic lutethium-177 (^{177}Lu)-loaded liposomes [176] (see also Section 4.3). Similarly, PET imaging has been used to quantify tumor uptake of mannose-coated liposomes radiolabeled with ^{64}Cu. Mannose coating was introduced to target tumor-associated macrophages, which was confirmed *ex vivo* by fluorescence microscopy using a fluorophore-labeled version of the liposomes [177].

Polymeric nanoparticles are gaining traction, both in preclinical development and in translational settings. Polymeric micelles can entrap small molecule drugs and act as carriers to tumors by passive accumulation. Researchers have frequently relied on nuclear imaging methods to evaluate polymeric nanoparticles' *in vivo* performance, either by labeling the polymeric matrix or the therapeutic payload. In a recent study, Zhang et al. developed a polymeric nanoparticle loaded with a porphyrin-containing drug that could be labeled with ^{64}Cu. Drug delivery was quantitatively monitored by PET in a mouse cancer model [178]. Porphyrin-polymer nanoparticles have also been proposed for photodynamic therapy (PDT). As mentioned above, porphyrin forms stable complexes with ^{64}Cu, which was exploited by Li et al. to build a multimodal imaging and therapeutic platform enabling monitored treatment of cancer [179]. Luo et al. used the same approach to non-invasively probe the biodistribution and tumor targeting of a doxorubicin-loaded poly(vinyl alcohol)-porphyrin nanoparticle by PET imaging at different time points after systemic administration in a mouse model of ovarian cancer [180].

The influence of targeting ligands on nanomedicines' *in vivo* behavior has been quantitatively evaluated by PET and SPECT. For instance, Andresen et al. evaluated the effect of coupling targeting ligands (octreotate) to ^{64}Cu-labeled liposomes on their pharmacokinetics and biodistribution by PET imaging. The presence of octreotate led to faster blood clearance and slightly lower neuroendocrine tumor accumulation compared to non-targeted liposomes [181]. In a similar fashion, nuclear imaging has been used to understand the behavior of inorganic nanoparticles applied for therapeutic payload delivery. PEGylated iron oxide nanoparticles, modified to carry doxorubicin and decorated with cyclo(Arg-Gly-Asp-D-Phe-Cys) (cRGDfC) for targeted delivery, were radiolabeled with ^{64}Cu to study the nanoparticles' *in vivo* fate by PET imaging [174] (Fig. 3D). The presence of targeting ligands resulted in increased tumor accumulation, as derived from the PET images. A similar result was obtained in a study using SPECT imaging to track intravenously administered ^{111}In-labeled sorafenib-loaded porous silicon nanoparticles decorated with an iRGD peptide [182].

In the literature, the theranostic approach, *i.e.* the combination of therapeutic and diagnostic payloads within the same nanocarrier, seems to be prevalent, but has little translational potential. This approach entails a good manufacturing practice (GMP) production for each individual theranostic companion imaging nanoparticle, and its respective approval for clinical use. Therefore, we introduced a novel concept whereby a non-therapeutic imaging nanoparticle, termed "nanoreporter", is co-injected along with a nanotherapeutic to provide quantitative information on the delivered dose in tumors [80] (Fig. 3E). Consequently, this does not require any chemical modification of the clinical-grade nanotherapeutic, which elevates the translational potential of the approach. Specifically, we co-injected empty ^{89}Zr-labeled liposomes and commercially available liposomal doxorubicin (Doxil®) in tumor-bearing mice and found that the PET imaging-derived quantitative information was predictive of therapy response, which indicates that this strategy could be used to identify patients amenable for nanotherapy. Moreover, we used the ^{89}Zr-liposome nanoreporter with other relevant nanoplatforms, such as PLGA nanoparticles and a nanoemulsion, and found an excellent correlation between the nanoreporter's' PET signal and the delivered nanotherapeutic dose. These findings imply that only a single nanoreporter would need to be approved for monitoring a wide range of nanomedicines. Interestingly, using ^{64}Cu-loaded liposomes, Lee et al. corroborated the nanoreporter approach and validated the predictive value of radiolabeled liposome uptake on treatment response [183].

While in general solid tumors are the targeted sites for nanomedicines, a growing number of studies report nuclear imaging-based assessment of targeting in other disease contexts. In a heart transplantation model, we were able to visualize ^{89}Zr-labeled, rapamycin-loaded HDL accumulation in the grafted tissue by PET imaging, indicative of incipient inflammation and efficient drug delivery to the targeted site. Importantly, we also derived quantitative evidence from the PET images of nanobiologic uptake in the bone marrow, which was critical for the tolerance effect observed [164]. Finally, a vaccine consisting of iron oxide nanoparticles carrying an antigen (ovalbumin) and a Toll-like receptor 9 agonist (CpG) was radiolabeled with ^{67}Ga, and SPECT imaging was used to demonstrate migration of the nanomaterial from the injection site to regional and nonregional lymph nodes [184].

4.3. Dosimetry

There are numerous studies reporting nanoplatforms as isotope carriers for radiotherapeutic purposes. These approaches typically rely on the enhanced accumulation of nanoparticles in tumors due to the EPR effect. In addition to pharmacokinetic and biodistribution data, these studies afford crucial information on dosimetry that can be used to adjust the administered dose for optimal response. Conveniently, the radiation of radiotherapeutic isotopes is typically accompanied by emission of gamma photons that can be detected by SPECT. For example, Ting et al. have exploited this feature using ^{188}Re-labeled liposomes for radiotherapy and detecting the concomitant 155-keV gamma photons to assess biodistribution and absorbed dose by SPECT [123–125]. Conversely, liposomes loaded with the β-emitter ^{177}Lu were used in a human xenograft mouse model and the authors used surrogate ^{64}Cu-loaded liposomes to extract *in vivo* information by PET imaging, including dosimetric data and tumor absorbed dose [176]. A similar surrogate PET imaging strategy was used to monitor a radiolabeled porphyrin-PEG nanoparticle formulation that was developed for dual photodynamic therapy and radiotherapy [119].

These imaging-based approaches have also been tested for other polymeric and inorganic nanoplatforms. For example, HPMA micelles have been labeled with ^{177}Lu [185] and ^{90}Y [186], using SPECT imaging in both studies to assess biodistribution. In the former study, the radiotherapeutic ^{177}Lu-labeled nanoparticle was used, whereas in the latter, a surrogate ^{111}In-labeled version of the nanomaterial had to be employed due to the absence of amenable gamma photons for SPECT imaging in ^{90}Y decay. In a similar fashion, SPECT has been employed for quantitative imaging-guided radiotherapy using iodine-131 (^{131}I)-labeled poly(cyclotriphosphazene-*co*-polyethylenimine) nanospheres [187] and poly(amidoamine) dendrimers [188] in murine cancer models. Radiolabeled gold nanoparticles, on the other hand, have been developed into nanoseeds for brachytherapy. Two recent studies reported the successful implementation of palladium-103 (^{103}Pd)- [189] and ^{177}Lu-labeled [117] gold nanoparticles for the treatment of solid tumors in mice. SPECT/CT imaging was used in both cases to longitudinally and quantitatively assess radioactivity retention after intratumoral implantation of the nanoseeds.

4.4. Nanoformulation integrity

Nanomedicines are mostly multicomponent materials consisting of a nanocarrier and a payload in the simplest scenario. The resulting nanomaterial is generally held together by non-covalent interactions, and therefore the construct's *in vivo* stability is of paramount importance for optimal performance. In this case, PET and SPECT imaging approaches have been tested to assess nanoformulations' integrity *in vivo*. This can be done sequentially, by radiolabeling different components of the same nanomaterial with the same isotope and evaluating their respective biodistribution in separate imaging experiments, or by radiolabeling the components with different isotopes for simultaneous imaging. We applied the former strategy to investigate the *in vivo* behavior of HDL nanoparticles by radiolabeling either its phospholipid load or its protein component (apolipoprotein 1, apoA-I) with ^{89}Zr [165]. Using PET imaging, we observed a significantly faster blood radioactivity clearance for phospholipid-labeled HDL compared to apoA-I-labeled HDL, which likely reflects *in vivo* phospholipid exchange with other lipoproteins and cell membranes and apoA-I's low cell internalization and catabolism.

A multi-isotope imaging approach can already be performed using SPECT scanners that can discriminate different gamma energy emissions, although multi-isotope PET imaging is also in development [39]. By way of example, following a dual-labeling approach Llop et al. used SPECT imaging to quantitatively assess the degradation of an albumin-stabilized PLGA nanoparticle *in vivo*. To this end, the polymer core was labeled with ^{111}In (γ energy: 173 and 247 keV), whereas the albumin coating was tagged with iodine-125 (^{125}I, γ energy: 35 keV). Imaging revealed a different tissue distribution for the two labels, suggesting a different fate for core and coating although deiodination could be a confounding factor [37]. A dual-isotope approach was also developed by Lamichhane et al. [190], who used ^{111}In-DTPA-liposomes encapsulating a ^{18}F-labeled carboplatin derivative. Analysis of the ^{111}In signal by SPECT and ^{18}F by PET using a multimodal pre-clinical PET/SPECT/CT system showed similar liver and spleen accumulation, indicating the stable integration of both.

Importantly, in addition to the valuable information obtained noninvasively by PET or SPECT, the use of nanoparticles labeled with gamma emitters also allows quantitative corroboration of the imaging results by highly sensitive *ex vivo* gamma counting. Most of the studies summarized in this section include this type of validation, showing tissue radioactivity distribution data that are in agreement with the imaging findings. Moreover, at this stage of development nanoparticles are frequently engineered to carry a fluorophore for complementary optical imaging. This dual-labeling approach covers the whole “resolution” range, as it allows quantitative evaluation of pharmacokinetics and biodistribution based on the radioactive tag at a whole-body level, and semiquantitative assessment of targeting at a tissue/cellular level by optical methods such as microscopy or fluorescence-activated cell sorting [167].

5. Nuclear imaging in translational nanomedicine research

In contrast to preclinical studies in mice, *ex vivo* radioactivity quantification in blood and tissues is challenging or unfeasible in larger animal models and patients. Therefore, translational and clinical studies depend on non-invasive imaging methods to provide relevant information on nanoparticle stability, tissue accumulation and therapy outcome *in vivo* [191]. Nuclear imaging is particularly suited for these applications, especially when combined with other modalities. For example, hybrid PET/MRI systems enable the visualization and quantification of radiotracers by PET in the detailed soft-tissue context generated by MRI [192–194]. In this section, we discuss how implementing these imaging approaches can benefit nanomedicine translation from small to larger animals. In addition, we highlight how nuclear imaging can be used to stratify patients and thereby improve nanomedicines' clinical evaluation.

5.1. Nanomedicine translation from small to large animal models

Nanomedicine development relies heavily on preclinical murine disease models with poor predictive value regarding therapeutic efficacy in larger animal models and humans. This explains, at least in part, why only a relatively low number of nanotherapeutics has received clinical approval. Particularly for cancer nanomedicine, murine orthotopic tumor models are the most common and, at the same time, the most criticized models due to their poor predictive value [20,195]. In addition to differences in pathophysiology, mouse hemodynamics, metabolic activity and immune responses are not exactly the same as in humans while these features critically influence nanomedicines' *in vivo* performance. Results from mouse studies certainly gain translational relevance if they can be replicated in larger animal models with (patho)physiological features more closely related to humans. In this setting, quantitative nuclear imaging approaches can aid nanomedicine translation by providing valuable *in vivo* information on: i) biodistribution and pharmacokinetic parameters over time in the same subject; ii) delivered doses to the target site for homogenizing patient cohorts; iii) treatment response assessed longitudinally. Simultaneously, implementing these approaches reduces the number of animals involved, which is necessary for ethical, logistical and economic reasons. Moreover, imaging studies involving large animals are also translationally relevant because they use clinical scanners and the implemented protocols can be readily adapted to humans. By doing so, studies in large animals also stimulate the transition from small-scale to medium- or large-scale nanotherapeutic production, which is essential for clinical translation and often overlooked during nanomedicine development [196].

For the evaluation of cancer nanomedicines, a noteworthy example of a preclinical model that resembles human pathophysiology and therefore offers predictive value involves dogs with spontaneous tumors (Fig. 4A). For example, Andresen et al. formulated ^{64}Cu-radiolabeled liposomes by remote loading and demonstrated the value of PET imaging in assessing tumor permeability heterogeneity in canine patients. The authors provided *in vivo* imaging evidence of EPR-based tumor accumulation in these animals, but importantly, also demonstrated that the effect differs vastly between solid tumors [175]. The same group also investigated the accelerated blood clearance effect in dogs [197]. This phenomenon is observed after repeated infusions of PEGylated materials, which leads to increased blood clearance rate due to the formation of anti-PEG antibodies [198]. The authors measured significantly shorter circulation half-lives for ^{64}Cu-labeled PEGylated liposomes in subsequent injections using PET, which could be partially prevented by increasing the first infusion's lipid dose or by administering a small pre-dose prior to the second injection [197]. These results not only have clear therapeutic implications, but also need to be taken into account for the implementation of theranostic approaches and patient selection strategies.

Nanomedicines have also been developed for anti-inflammatory treatment of atherosclerosis [199]. In this setting, quantitative imaging-based screening procedures would be tremendously valuable to homogenize patient populations and identify likely responders. To that end, we developed a highly translational PET/MR imaging protocol to quantify the uptake of liposomes in the arterial wall of rabbits [200]. Specifically, ^{89}Zr labeling allowed us to quantify liposomal uptake by PET, whereas MRI's excellent soft-tissue contrast and spatial resolution provided vessel wall anatomical reference. Images showed a patchy distribution of radioactivity along the aorta of rabbits with atherosclerosis, which was corroborated by *ex vivo* autoradiography. Importantly, gamma counting of aortic

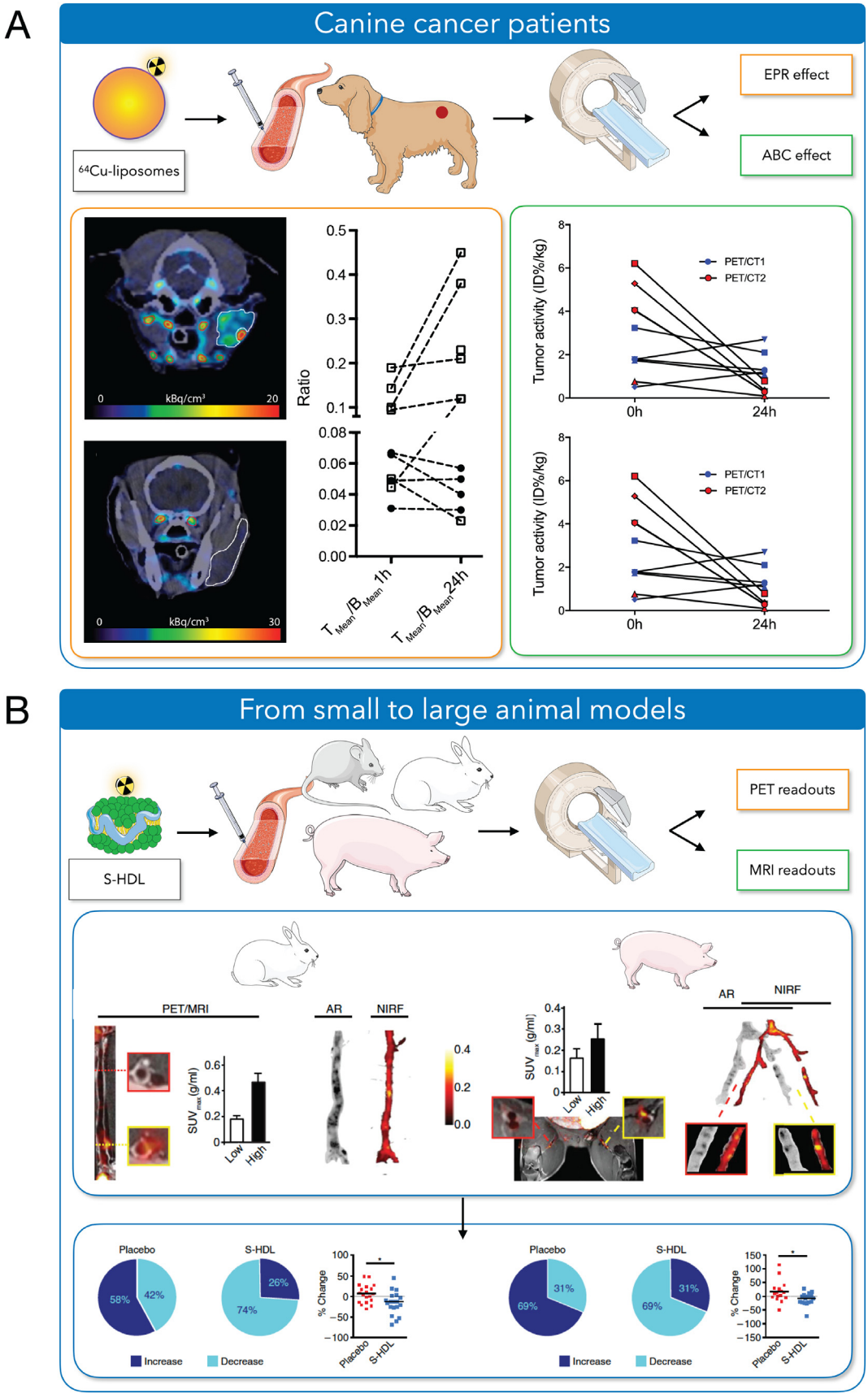
A
Canine cancer patients
64Cu-liposomes
EPR effect
ABC effect
0
kBq/cm³
20
0
kBq/cm³
30
Ratio
0.5
0.4
0.3
0.2
0.1
0.08
0.06
0.04
0.02
0.00
T Mean /B Mean 1h
T Mean /B Mean 24h
Tumor activity (ID%/kg)
PET/CT1
PET/CT2
0h
24h
B
From small to large animal models
S-HDL
PET readouts
MRI readouts
PET/MRI
AR
NIRF
SUV max (g/ml)
Low
High
Placebo
S-HDL
58%
42%
74%
26%
69%
31%
Increase
Decrease
% Change

samples confirmed the imaging results, indicating that liposomal uptake in the vessel wall can be accurately quantified using PET imaging.

This imaging approach was also used in a recent study, where we demonstrated the scale-up of simvastatin-loaded HDL (S-HDL), and its evaluation in murine rabbit and porcine atherosclerosis models (Fig. 4B) [153]. In this study, we integrated PET imaging at two translational stages. First, we used PET/CT to evaluate the biodistribution and pharmacokinetics of ^{89}Zr-labeled S-HDL. Its plaque targeting ability was assessed by PET/MRI, which allows a clear delineation of the vessel wall. Radioactivity distribution was very similar in the murine, rabbit and porcine atherosclerosis models, indicating a similar *in vivo* performance. Second, we implemented a multiparametric PET/MR imaging protocol to longitudinally evaluate treatment response in rabbits and pigs. Specifically, we used two PET radiotracers, namely ^{18}F-labeled 2-deoxy-2-fluoro-D-glucose (^{18}F-FDG) and 3′-deoxy-3′-fluorothymidine (^{18}F-FLT), to quantitatively assess vessel wall inflammation and cellular proliferation, respectively, in addition to MRI-based vessel wall thickness and permeability measurements. This approach allowed us to derive quantitative information on four imaging markers of atherosclerosis progression. In doing so, we could perform these experiments using the relatively few large animals that could reasonably be included. We found consistent anti-inflammatory efficacy of simvastatin-HDL in all three animal models of atherosclerosis, supporting the translatability of the approach and its potential to treat atherosclerosis [153].

In another study focused on atherosclerosis treatment, we reported the development of an immunomodulating TNF receptor-associated factor 6 inhibitor-loaded HDL (TRAF6i-HDL) nanobiologic and its evaluation in multiple species [81]. After comprehensive evaluation in atherosclerotic *Apoe*$^{-/-}$ mice, we performed extensive toxicity and biodistribution studies in non-human primates. Using ^{89}Zr-labeled TRAF6i-HDL, we longitudinally imaged radioactivity distribution by PET/MRI, first dynamically over the 60 min after intravenous administration, then statically at 24, 48 and 72 h. We observed rapid accumulation in the liver, spleen and kidneys, followed by a significant uptake in the bone marrow. At 24, 48 and 72 h, radioactivity was found mostly in the liver and spleen. These *in vivo* data were corroborated by *ex vivo* gamma counting of tissue samples. Interestingly, the overall organ distribution of ^{89}Zr-TRAF6i-HDL was similar in mice and non-human primates. In a similar fashion, we performed translational PET/MR imaging of a hyaluronan nanotherapeutic in rabbits with atherosclerosis to determine the nanoparticles' biodistribution, pharmacokinetics and plaque targeting efficiency for 24 h. We were able to visualize and quantify blood clearance and tissue distribution through dynamic PET imaging over the first 60 min after administration and measured high plaque-to-muscle ratios indicative of specific accumulation in these lesions [201].

5.2. Clinical nanomedicine studies

While (nuclear) imaging is firmly embedded in preclinical nanomedicine research, its role in clinical studies is much less pronounced (reviewed by Man et al. [191]). This is remarkable, given the fact that nuclear imaging is non-invasive and can provide quantitative information predictive of nanomedicines' therapeutic efficacy. Particularly in the oncology field, where clinical evaluation of novel targeted therapies is commonly supported by biomarker quantification and companion diagnostics, it is surprising this is not as yet standard practice for cancer nanomedicine implementation. Most nanomedicines are being developed for treatment of solid tumors and, as such, rely heavily on the EPR effect for therapeutic efficacy. Although it is clear that the EPR effect is much more pronounced in preclinical xenograft tumor models [202], it has been convincingly demonstrated in human cancer patients, albeit with high inter- and intra-patient and tumor variability. Therefore, in addition to tissue and liquid biomarkers, many efforts are currently directed at the development of non-invasive imaging methods to probe the EPR profile in individual patients (Fig. 5) [1]. Ultimately, these strategies can be implemented in the cancer staging/diagnostic routine or therapeutic regimen and will aid patient selection and therapy outcome prediction.

Pioneering studies used ^{111}In- or ^{99m}Tc-radiolabeling to determine the safety and ability of empty liposomes to detect tumors, observing the EPR effect in humans for the first time [191,203–205]. Later on, others provided valuable insights into the *in vivo* behavior of PEGylated 'stealth' liposomes. The scintigraphy images published by Harrington and colleagues remain one of the most impressive representations of the EPR effect in human tumors [206,207]. The first clinical studies involving imaging of ^{99m}Tc-radiolabeled liposomes containing a therapeutic payload were conducted by Koukourakis et al. [208,209]. Nuclear imaging has been also used to demonstrate the EPR effect enhancement by local hyperthermia by Kleiter et al. [210]. Scintigraphy and SPECT measurements showed an increased ^{99m}Tc accumulation in heated tumors which correlated well with HPLC measurements of intratumoural doxorubicin. More recently, theranostic approaches have used other radiolabels (*e.g.*, ^{64}Cu) to evaluate the relation between the EPR effect and nanomedicines' therapeutic efficacy in patients. The most compelling recent example of a clinical study using this approach has been reported by Lee et al. from Merrimack Pharmaceuticals [211]. During a phase I dose-escalation study to determine the safety of HER2-targeted liposomal doxorubicin (MM-302) in patients with HER2-positive metastatic breast cancer [212], the EPR effect was assessed by PET/CT following systemic administration of ^{64}Cu-labeled MM-302. The authors reported highly variable levels (35-fold) of MM-302 tumor accumulation (0.52–18.5%ID/kg). Importantly, retrospective analysis revealed the relation between a high MM-302 tumor deposition, and more favorable treatment outcomes (Fig. 5).

Fig. 4. Nuclear imaging enables the evaluation of nanomedicines in larger animal models. **A**) Canine patients with spontaneous tumors to assess cancer nanomedicines. *Top*. PET/CT imaging can be used to determine pharmacokinetic parameters and biodistribution of ^{64}Cu-radiolabeled liposomes following intravenous administration. *Bottom left*. Heterogeneous tumor uptake of liposomes 24 h after systemic administration in a canine patient with adenocarcinoma (*top*) and soft tissue sarcoma (*bottom*). Tumors are delineated by white lines. *Bottom middle*. Liposome tumor-to-reference tissue activity ratios. Tumor mean to blood mean (*T*mean / *B*mean) activity ratios on 1-h and 24-h PET scans following systemic administration in 10 canine patients with spontaneous tumor demonstrating enhanced permeability and retention (EPR) effect heterogeneity. Reprinted (adapted) with permission from Hansen et al. [175]. Copyright 2015 American Chemical Society. *Bottom right*. Repeated ^{64}Cu-liposome PET/CT scans induce accelerated blood clearance (ABC) effect in canine cancer patients. Tumor %ID/kg mean activity at 24 h from 2 PET/CT scans for five dogs. Reprinted (adapted) with permission from Børresen et al. [197]. Copyright 2018 American Chemical Society. **B)** Small and large animal models to evaluate a nanoimmunotherapy for atherosclerosis. *Top*. PET/CT and PET/MRI can be used to determine pharmacokinetic parameters, biodistribution and therapeutic effect of a simvastatin-loaded high-density lipoprotein (S-HDL) nanotherapeutic. *Middle*. PET/MRI assessment of plaque targeting and quantification of standardized uptake values (SUVs) in one rabbit (top) and one pig (bottom), 48 h after injection of [^{89}Zr]-S-HDL, in the low and high uptake regions shown in the red- and yellow-bordered squares, respectively. Regional distribution of S-HDL in atherosclerotic samples from rabbits (*left*) and pigs (*right*), as determined by autoradiography (AR; [^{89}Zr]-S-HDL) and near-infrared fluorescence (NIRF; DiD-S-HDL) 48 h after injection. *Bottom left*. Proportion of scans that afforded increased or decreased imaging marker values in rabbits treated with PBS (placebo) or S-HDL and pooled representation of the variation in the four independent imaging parameters (line is situated at median). *Bottom right*. Proportion of scans that afforded increased or decreased imaging marker values in pigs treated with PBS (placebo) or S-HDL and pooled representation of the variation in the four independent imaging parameters (line is situated at median, right). Reprinted (adapted) with permission from Binderup et al. [153]. Copyright 2019 American Association for the Advancement of Science.

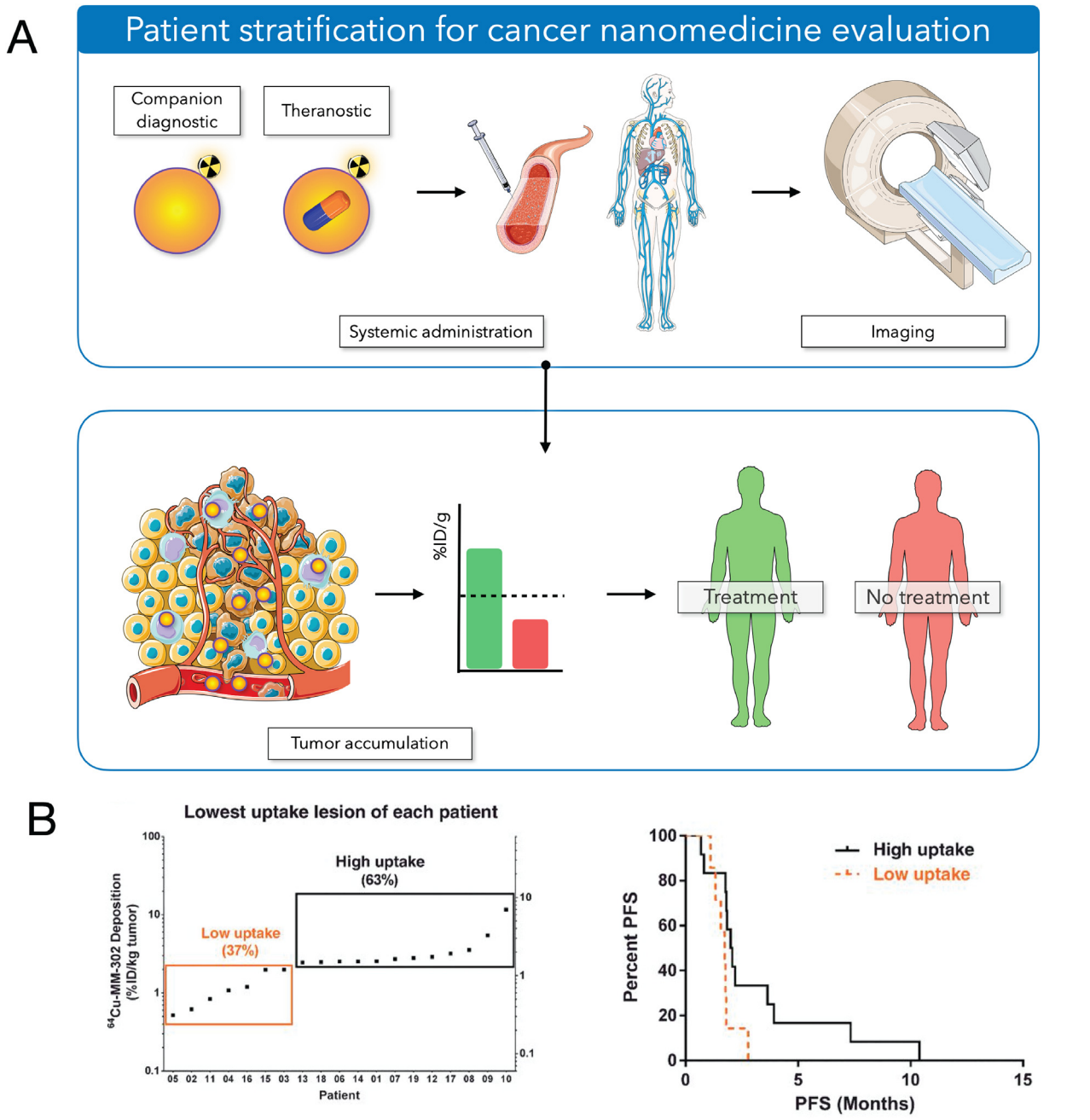

Fig. 5. Schematic overview of patient stratification strategies for cancer nanomedicine evaluation. **A**) The tumor accumulation of companion diagnostic nanoparticles or theranostic nanomedicines can be determined using quantitative (nuclear) imaging techniques after systemic administration. Based on the percentage of the nanoparticle's injected dose per gram of tumor tissue (%ID/g), patients can be selected who will most likely benefit from treatment. **B**) The tumor accumulation (%ID/kg tumor) of ^{64}Cu-labeled liposomes containing doxorubicin and targeted to HER2 (MM-302) was predictive for their therapeutic efficacy measured by patients' progression free survival (PFS). Reprinted (adapted) with permission from Lee et al. [211]. Copyright 2017 American Association for Cancer Research.

Recently, another strategy is receiving considerable attention. As discussed in Section 4.2, a nanomedicine's tumor accumulation can be derived from nuclear imaging-based quantification of a non-therapeutic radiolabeled nanoreporter's signal [80]. These radiolabeled companion diagnostic nanoparticles provide both spatial and quantitative information on nanotherapeutics with similar physicochemical characteristics. While we and others have demonstrated the validity of this approach in preclinical proof-of-concept studies [80,183], it is readily translatable to larger animal models or human patients. For example, Giovinazzo et al. investigated Doxil® biodistribution using companion ^{99m}Tc-sulfur colloid in women with ovarian cancer [213]. The authors demonstrated a strong correlation between blood levels of ^{99m}Tc and doxorubicin determined by scintigraphy and HPLC, respectively. Subsequently, they could estimate doxorubicin levels based on the imaging signal. They found a positive and significant correlation between palmar-plantar erythrodysesthesia (hand-foot syndrome) toxicity and estimated doxorubicin concentration in hands. In a similar fashion, MRI-based companion diagnostics approaches to guide nanomedicine development have also been reported. The most compelling study so far has been reported by Ramanathan et al., who used FDA-approved 30 nm iron oxide nanoparticles (ferumoxytol, Feraheme®) as a companion diagnostic to predict treatment response of liposomal irinotecan (Onivyde®) in patients with advanced solid tumors [214]. Ferumoxytol levels were quantified by T2* MRI while irinotecan levels were

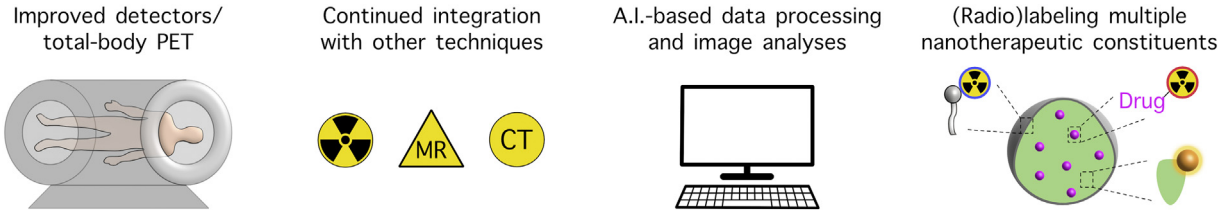

Fig. 6. Schematic overview of expected advances in nuclear imaging and radiolabeling that will benefit the clinical translation of nanotherapeutics. These include improved detectors and total-body PET, continued hybridization with other imaging techniques, artificial intelligence (A.I.)-based data analyses, and the orthogonal (radio)labeling of multiple nanotherapeutic components.

determined in patient biopsies. Results showed that higher levels of ferumoxytol tumor accumulation correlated with greater reductions in lesion size following Onivyde® treatment. While the advantages of MRI include its cost-effectiveness, spatial resolution and the lack of ionizing radiation, it is more challenging to accurately quantify signals from contrast agents. In addition, MRI requires imaging before and after administration of the contrast agent, further complicating the analysis.

Finally, Phillips et al. demonstrated the feasibility of integrating quantitative PET imaging readouts for the assessment of a nanomedicine's *in vivo* behavior in humans [215]. In a pilot clinical trial, the authors radiolabeled a small (6–7 nm) core-shell hybrid silica nanoparticle with ^{124}I to quantitatively assess biodistribution and pharmacokinetics in a small group of human subjects over a period of three days. PET images were used to longitudinally measure clearance kinetics and accumulation in tissues and confirmed renal excretion due to the nanoparticles' small size. Importantly, the generated information was also used to derive radiation dosimetry data.

6. Conclusions and perspective

Nuclear imaging's quantitative nature, its practically unlimited penetration depth and high sensitivity make it exceptionally suited to non-invasively investigate nanotherapeutics *in vivo* [24,191,216]. However, these techniques are not devoid of limitations. PET and SPECT provide no anatomical reference, have only moderate spatial resolution compared to MRI [217], expose the patient to radiation, are relatively expensive and present operational challenges (*e.g.*, the 109-min physical half-life of ^{18}F requires a nearby cyclotron for routine production).

In recent decades, novel scintillator materials and photodetector designs have led to major increases in sensitivity and timing resolution [217,218]. Given the favorable properties of current digital silicon photomultipliers (*e.g.*, their small size and magnetic insusceptibility) it is likely that fully digital detectors will become the norm [217,218]. Apart from improvements in detector design, the number of detectors per scanner has been steadily increasing. This has recently resulted in the first total-body PET scanner, with unprecedented resolution and sensitivity [219]. This development is especially relevant for nanomedicine translation, where fast total-body imaging is required to fully capture nanotherapeutics' pharmacokinetics and biodistribution. Related, enhancements in sensitivity and resolution will allow extended longitudinal experiments. We therefore expect dynamic total-body PET imaging to play a vital role in the future translation of nanotherapeutics (Fig. 6).

The integration of PET and SPECT with other imaging modalities will likely also continue [220–223]. PET/CT and SPECT/CT have allowed overlying nuclear imaging (functional) data with anatomical information, and combinations of PET with MRI [224] or optical techniques [225] provide soft-tissue contrast and enhanced resolution. Such hybrid techniques will greatly benefit assessing nanomedicines' *in vivo* stability and tissue-specific uptake, for example by visualizing their accumulation in atherosclerotic plaques using PET/MRI [30,226]. Besides complementing nuclear imaging data, these hybrid approaches facilitate improving nuclear imaging's quantitative ability through advanced data processing (*e.g.*, by using anatomical CT and MRI data to correct PET images for attenuation [227], or partial volume effects) [228]. Importantly, these advancements in both stand-alone and hybrid nuclear imaging techniques also greatly increase the amount of data produced. Processing data using artificial intelligence has tremendous potential in increasing resolution, accelerating image reconstruction, reducing artifacts, and identifying tissues of interest [229–232]. Although still barely investigated, we expect machine learning to also facilitate the simultaneous *in vivo* screening of multiple nanotherapeutic formulations, thereby greatly accelerating their development [233–236].

Nuclear imaging's relevance to nanotherapeutic translation will also depend on developments in radiolabeling strategies. Current approaches often rely on post-formulation chelation of radionuclides, which leaves the radionuclide on the nanotherapeutics' exterior and thereby susceptible to interactions with other compounds [24,81,216,237]. More important, this strategy provides only minimal insight into nanocarrier integrity and *in vivo* drug retention. To obtain such insight – and facilitate quantitative multimodal imaging – approaches in which multiple nanotherapeutic constituents are orthogonally (radio)labeled are highly desirable [238]. This approach's feasibility has already been demonstrated using dual-radionuclide SPECT imaging [36,37], and similar PET methodologies are in early stages of development [239,240]. The increasing availability of high-quality preclinical PET/SPECT and PET/SPECT/CT scanners will further facilitate multi-isotope nuclear imaging [241]. However, employing multiple radiolabels increases patients' exposure to radiation and concomitant efforts to reduce the required doses are therefore highly desirable. Furthermore, as introducing multiple (radio) labels increases the risk of altering nanotherapeutics' properties, this should ideally proceed through minimally interfering strategies *e.g.*, by replacing a carbon atom in the drug with radioactive ^{11}C instead of functionalizing it with a chelator. Although a detailed description of the factors influencing nanocarriers' *in vivo* specificity is beyond the scope of this review, improving tissue selectivity represents another way to boost nuclear imaging's efficacy (*e.g.*, improved tumor uptake will enhance contrast with healthy tissue).

Combined, we expect nanomedicine translation to benefit from advances in dynamic total-body nuclear imaging, including detector design and data processing. Although non-nuclear and semi-quantitative imaging approaches are being developed [242,243], we foresee that hybrid techniques will become increasingly important. Lastly, a continued effort towards multimodal-(radio)labeling approaches will improve insight into nanotherapeutics' *in vivo* stability, guaranteeing nuclear imaging's relevance to nanotherapeutic translation for years to come [37].

Acknowledgements

The work of EK, RvdM and WJMM is supported by the Dutch Research Council (NWO; ZonMW Vici grant no. 016.176.622 to WJMM). CPM is supported by Comunidad Autónoma de Madrid's Programa de Atracción de Talento (2018 T1/BMD10758).

References

[1] R. Van der Meel, E. Sulheim, Y. Shi, F. Kiessling, W.J.M.M. Mulder, T. Lammers, Smart cancer nanomedicine, Nat. Nanotechnol. 14 (2019) 1007–1017, https://doi.org/10.1038/s41565-019-0567-y.

[2] B. Pelaz, C. Alexiou, R.A. Alvarez-Puebla, F. Alves, A.M. Andrews, S. Ashraf, L.P. Balogh, L. Ballerini, A. Bestetti, C. Brendel, S. Bosi, M. Carril, W.C.W. Chan, C. Chen, X. Chen, X. Chen, Z. Cheng, D. Cui, J. Du, C. Dullin, A. Escudero, N. Feliu, M. Gao, M. George, Y. Gogotsi, A. Grünweller, Z. Gu, N.J. Halas, N. Hampp, R.K. Hartmann, M.C. Hersam, P. Hunziker, J. Jian, X. Jiang, P. Jungebluth, P. Kadhiresan, K. Kataoka, A. Khademhosseini, J. Kopeček, N.A. Kotov, H.F. Krug, D.S. Lee, C.M. Lehr, K.W. Leong, X.J. Liang, M.L. Lim, L.M. Liz-Marzán, X. Ma, P. Macchiarini, H. Meng, H. Möhwald, P. Mulvaney, A.E. Nel, S. Nie, P. Nordlander, T. Okano, J. Oliveira, T.H. Park, R.M. Penner, M. Prato, V. Puntes, M. Rotello, A. Samarakoon, R.E. Schaak, Y. Shen, S. Sjöqvist, A.G. Skirtach, M.G. Soliman, M.M. Stevens, H.W. Sung, B.Z. Tang, R. Tietze, B.N. Udugama, J. Scott, T. VanEpps, P.S. Weil, I. Weiss, Y. Wu Willner, L. Yang, Z. Yue, Q. Zhang, Q. Zhang, X.E. Zhang, Y. Zhao, X. Zhou, W.J. Parak, Diverse applications of nanomedicine, ACS Nano 11 (2017) 2313–2381, https://doi.org/10.1021/acsnano.6b06040.

[3] J.E. Lancet, G.L. Uy, J.E. Cortes, L.F. Newell, T.L. Lin, E.K. Ritchie, R.K. Stuart, S.A. Strickland, D. Hogge, S.R. Solomon, R.M. Stone, D.L. Bixby, J.E. Kolitz, G.J. Schiller, M.J. Wieduwilt, D.H. Ryan, A. Hoering, K. Banerjee, M. Chiarella, A.C. Louie, B.C. Medeiros, CPX-351 (cytarabine and daunorubicin) liposome for injection versus conventional cytarabine plus daunorubicin in older patients with newly diagnosed secondary acute myeloid leukemia, J. Clin. Oncol. 36 (2018) 2684–2692, https://doi.org/10.1200/JCO.2017.77.6112.

[4] A.C. Krauss, X. Gao, L. Li, M.L. Manning, P. Patel, W. Fu, K.G. Janoria, G. Gieser, D.A. Bateman, D. Przepiorka, Y.L. Shen, S.S. Shord, C.M. Sheth, A. Banerjee, J. Liu, K.B. Goldberg, A.T. Farrell, G.M. Blumenthal, R. Pazdur, FDA approval summary: (daunorubicin and cytarabine) liposome for injection for the treatment of adults with high-risk acute myeloid leukemia, Clin. Cancer Res. 25 (2019) 2685–2690, https://doi.org/10.1158/1078-0432.CCR-18-2990.

[5] Y. Dong, D.J. Siegwart, D.G. Anderson, Strategies, design, and chemistry in siRNA delivery systems, Adv. Drug Deliv. Rev. 144 (2019) 133–147, https://doi.org/10.1016/J.ADDR.2019.05.004.

[6] D. Adams, A. Gonzalez-Duarte, W.D. O, C.C. Riordan, M. Yang, A.V. Ueda, I. Kristen, H.H. Tournev, T. Schmidt, J.L. Coelho, K.P. Berk, G. Lin, S. Vita, V. Attarian, M.M. Plante-Bordeneuve, J.M. Mezei, J. Campistol, T.H. Buades, B.J. Brannagan 3rd, J.Oh. Kim, Y. Parman, Y. Sekijima, P.N. Hawkins, S.D. Solomon, M. Polydefkis, P.J. Dyck, P.J. Gandhi, S. Goyal, J. Chen, A.L. Strahs, S.V. Nochur, M.T. Sweetser, P.P. Garg, A.K. Vaishnaw, J.A. Gollob, O.B. Suhr, T.H. Brannagan 3rd, B.J. Kim, J. Oh, Y. Parman, Y. Sekijima, P.N. Hawkins, S.D. Solomon, M. Polydefkis, P.J. Dyck, P.J. Gandhi, S. Goyal, J. Chen, A.L. Strahs, S.V. Nochur, M.T. Sweetser, P.P. Garg, A.K. Vaishnaw, J.A. Gollob, O.B. Suhr, Patisiran, an RNAi therapeutic, for hereditary transthyretin amyloidosis, N. Engl. J. Med. 379 (2018) 11–21, https://doi.org/10.1056/NEJMoa1716153.

[7] A. Akinc, M.A. Maier, M. Manoharan, K. Fitzgerald, M. Jayaraman, S. Barros, S. Ansell, X. Du, M.J. Hope, T.D. Madden, B.L. Mui, S.C. Semple, Y.K. Tam, M. Ciufolini, D. Witzigmann, J.A. Kulkarni, R. van der Meel, P.R. Cullis, The Onpattro® story and the clinical translation of nanomedicines containing nucleic acid-based drugs, Nat. Nanotechnol. 14 (2019) 1084–1087, https://doi.org/10.1038/s41565-019-0591-y.

[8] Q. Sun, M. Barz, B.G. De Geest, M. Diken, W.E. Hennink, F. Kiessling, T. Lammers, Y. Shi, Nanomedicine and macroscale materials in immuno-oncology, Chem. Soc. Rev. 48 (2019) 351–381, https://doi.org/10.1039/c8cs00473k.

[9] W.J.M. Mulder, J. Ochando, L.A.B. Joosten, Z.A. Fayad, M.G. Netea, Therapeutic targeting of trained immunity, Nat. Rev. Drug Discov. 18 (2019) 553–566, https://doi.org/10.1038/s41573-019-0025-4.

[10] W. Jiang, C.A. von Roemeling, Y. Chen, Y. Qie, X. Liu, J. Chen, B.Y.S. Kim, Designing nanomedicine for immuno-oncology, Nat. Biomed. Eng. 1 (2017) https://doi.org/10.1038/s41551-017-00290029.

[11] R.S. Riley, C.H. June, R. Langer, M.J. Mitchell, Delivery technologies for cancer immunotherapy, Nat. Rev. Drug Discov. 18 (2019) 175–196, https://doi.org/10.1038/s41573-018-0006-z.

[12] D.J. Irvine, E.L. Dane, Enhancing cancer immunotherapy with nanomedicine, Nat. Rev. Immunol. 20 (2020) 321–334, https://doi.org/10.1038/s41577-019-0269-6.

[13] J.I. Hare, T. Lammers, M.B. Ashford, S. Puri, G. Storm, S.T. Barry, Challenges and strategies in anti-cancer nanomedicine development: an industry perspective, Adv. Drug Deliv. Rev. 108 (2017) 25–38, https://doi.org/10.1016/j.addr.2016.04.025.

[14] Y. Matsumura, H. Maeda, A new concept for macromolecular therapeutics in Cancer chemotherapy: mechanism of Tumoritropic accumulation of proteins and the antitumor agent Smancs, Cancer Res. 46 (1986) 6387–6392.

[15] H. Maeda, Toward a full understanding of the EPR effect in primary and metastatic tumors as well as issues related to its heterogeneity, Adv. Drug Deliv. Rev. 91 (2015) 3–6, https://doi.org/10.1016/J.ADDR.2015.01.002.

[16] Y. Barenholz, Doxil?? - the first FDA-approved nano-drug: lessons learned, J. Control. Release 160 (2012) 117–134, https://doi.org/10.1016/j.jconrel.2012.03.020.

[17] S. Wilhelm, A.J. Tavares, Q. Dai, S. Ohta, J. Audet, H.F. Dvorak, W.C.W. Chan, Analysis of nanoparticle delivery to tumours, Nat. Rev. Mater. 1 (2016) 16014, https://doi.org/10.1038/natrevmats.2016.14.

[18] S. Sindhwani, A.M. Syed, J. Ngai, B.R. Kingston, L. Maiorino, J. Rothschild, P. MacMillan, Y. Zhang, N.U. Rajesh, T. Hoang, J.L.Y. Wu, S. Wilhelm, A. Zilman, S. Gadde, A. Sulaiman, B. Ouyang, Z. Lin, L. Wang, M. Egeblad, W.C.W. Chan, The entry of nanoparticles into solid tumours, Nat. Mater. 19 (2020) 566–575, https://doi.org/10.1038/s41563-019-0566-2.

[19] Z. Cheng, A. Al Zaki, J.Z. Hui, V.R. Muzykantov, A. Tsourkas, Multifunctional nanoparticles: cost versus benefit of adding targeting and imaging capabilities, Science. 338 (2012) 903–910, https://doi.org/10.1126/science.1226338.

[20] M. Björnmalm, K.J. Thurecht, M. Michael, A.M. Scott, F. Caruso, Bridging bio-nano science and cancer nanomedicine, ACS Nano 11 (2017) 9594–9613, https://doi.org/10.1021/acsnano.7b04855.

[21] T.S.C. Ng, M.A. Garlin, R. Weissleder, M.A. Miller, Improving nanotherapy delivery and action through image-guided systems pharmacology, Theranostics. 10 (2020) 968–997, https://doi.org/10.7150/thno.37215.

[22] C. Pérez-Medina, S. Hak, T. Reiner, Z.A. Fayad, M. Nahrendorf, W.J.M. Mulder, Integrating nanomedicine and imaging, Philos. Trans. R. Soc. A Math. Phys. Eng. Sci. 375 (2017) https://doi.org/10.1098/rsta.2017.011020170110.

[23] M.L. Senders, Z.A. Fayad, T. Reiner, W.J. Mulder, C. Pérez-Medina, Imaging-guided revival of nanomedicine? Nanomedicine. 12 (2017) 89–90, https://doi.org/10.2217/nnm-2016-0365.

[24] F. Man, P.J. Gawne, R. T.M. de Rosales, Nuclear imaging of liposomal drug delivery systems: a critical review of radiolabelling methods and applications in nanomedicine, Adv. Drug Deliv. Rev. 143 (2019) 134–160, https://doi.org/10.1016/J.ADDR.2019.05.012.

[25] L. Papp, C.P. Spielvogel, I. Rausch, M. Hacker, T. Beyer, Personalizing medicine through hybrid imaging and medical big data analysis, Front. Phys. 6 (2018) 51, https://doi.org/10.3389/fphy.2018.00051.

[26] P. Lambin, R.T.H. Leijenaar, T.M. Deist, J. Peerlings, E.E.C. De Jong, J. Van Timmeren, S. Sanduleanu, R.T.H.M. Larue, A.J.G. Even, A. Jochems, Y. Van Wijk, H. Woodruff, J. Van Soest, T. Lustberg, E. Roelofs, W. Van Elmpt, A. Dekker, F.M. Mottaghy, J.E. Wildberger, S. Walsh, Radiomics: the bridge between medical imaging and personalized medicine, Nat. Rev. Clin. Oncol. 14 (2017) 749–762, https://doi.org/10.1038/nrclinonc.2017.141.

[27] D.P. Cormode, E. Roessl, A. Thran, T. Skajaa, R.E. Gordon, J.-P. Schlomka, V. Fuster, E.A. Fisher, W.J.M. Mulder, R. Proksa, Z.A. Fayad, Atherosclerotic plaque composition: analysis with multicolor CT and targeted gold nanoparticles, Radiology. 256 (2010) 774–782, https://doi.org/10.1148/radiol.10092473.

[28] I. Tirotta, V. Dichiarante, C. Pigliacelli, G. Cavallo, G. Terraneo, F.B. Bombelli, P. Metrangolo, G. Resnati, 19F magnetic resonance imaging (MRI): from design of materials to clinical applications, Chem. Rev. 115 (2015) 1106–1129, https://doi.org/10.1021/cr500286d.

[29] A.A. Kislukhin, H. Xu, S.R. Adams, K.H. Narsinh, R.Y. Tsien, E.T. Ahrens, Paramagnetic fluorinated nanoemulsions for sensitive cellular fluorine-19 magnetic resonance imaging, Nat. Mater. 5 (2016) 662–668, https://doi.org/10.1038/nmat4585.

[30] M.L. Senders, A.E. Meerwaldt, M.M.T. van Leent, B.L. Sanchez-Gaytan, J.C. van de Voort, Y.C. Toner, A. Maier, E.D. Klein, N.A.T. Sullivan, A.M. Sofias, H. Groenen, C. Faries, R.S. Oosterwijk, E.M. van Leeuwen, F. Fay, E. Chepurko, T. Reiner, R. Duivenvoorden, L. Zangi, R.M. Dijkhuizen, S. Hak, F.K. Swirski, M. Nahrendorf, C. Pérez-Medina, A.J.P. Teunissen, Z.A. Fayad, C. Calcagno, G.J. Strijkers, W.J.M. Mulder, Probing myeloid cell dynamics in ischaemic heart disease by nanotracer hot-spot imaging, Nat. Nanotechnol. 15 (2020) 398–405, https://doi.org/10.1038/s41565-020-0642-4.

[31] A.J.P. Teunissen, C. Pérez-Medina, A. Meijerink, W.J.M. Mulder, Investigating supramolecular systems using Förster resonance energy transfer, Chem. Soc. Rev. 47 (2018) 7027–7044, https://doi.org/10.1039/c8cs00278a.

[32] B.L. Sanchez-Gaytan, F. Fay, S. Hak, A. Alaarg, Z.A. Fayad, C. Pérez-Medina, W.J.M. Mulder, Y. Zhao, Real-time monitoring of nanoparticle formation by FRET imaging, Angew. Chem. Int. Ed. 56 (2017) 2923–2926, https://doi.org/10.1002/anie.201611288.

[33] Y. Zhao, I. van Rooy, S. Hak, F. Fay, J. Tang, C. de L. Davies, M. Skobe, E.A. Fisher, A. Radu, Z.A. Fayad, C. de Mello Donegá, A. Meijerink, W.J.M. Mulder, Near-infrared fluorescence energy transfer imaging of nanoparticle accumulation and dissociation kinetics in tumor-bearing mice, ACS Nano 7 (2013) 10362–10370, https://doi.org/10.1021/nn404782p.

[34] D.L. Bailey, K.P. Willowson, Quantitative SPECT/CT: SPECT joins PET as a quantitative imaging modality, Eur. J. Nucl. Med. Mol. Imaging 41 (2014) 17–25, https://doi.org/10.1007/s00259-013-2542-4.

[35] W.G. Kreyling, A.M. Abdelmonem, Z. Ali, F. Alves, M. Geiser, N. Haberl, R. Hartmann, S. Hirn, D.J. de Aberasturi, K. Kantner, G. Khadem-Saba, J.-M. Montenegro, J. Rejman, T. Rojo, I.R. de Larramendi, R. Ufartes, A. Wenk, W.J. Parak, In vivo integrity of polymer-coated gold nanoparticles, Nat. Nanotechnol. 10 (2015) 619–623, https://doi.org/10.1038/nnano.2015.111.

[36] K.C.L. Black, W.J. Akers, G. Sudlow, B. Xu, R. Laforest, S. Achilefu, Dual-radiolabeled nanoparticle SPECT probes for bioimaging, Nanoscale. 7 (2015) 440–444, https://doi.org/10.1039/C4NR05269B.

[37] J. Llop, P. Jiang, M. Marradi, V. Gómez-Vallejo, M. Echeverría, S. Yu, M. Puigivila, Z. Baz, B. Szczupak, C. Pérez-Campaña, Z. Mao, C. Gao, S.E. Moya, Visualisation of dual radiolabelled poly(lactide-co-glycolide) nanoparticle degradation in vivo using energy-discriminant SPECT, J. Mater. Chem. B 3 (2015) 6293–6300, https://doi.org/10.1039/C5TB01157D.

[38] A. Andreyev, A. Celler, Dual-isotope PET using positron-gamma emitters, Phys. Med. Biol. 56 (2011) 4539–4556, https://doi.org/10.1088/0031-9155/56/14/020.

[39] T. Fukuchi, T. Okauchi, M. Shigeta, S. Yamamoto, Y. Watanabe, S. Enomoto, Positron emission tomography with additional γ -ray detectors for multiple-tracer imaging, Med. Phys. 44 (2017) 2257–2266, https://doi.org/10.1002/mp.12149.

[40] W.J.M. Mulder, F.A. Jaffer, Z.A. Fayad, M. Nahrendorf, Imaging and nanomedicine in inflammatory atherosclerosis, Sci. Transl. Med. 6 (2014) 239sr1, https://doi.org/10.1126/scitranslmed.3005101.

[41] Y. Xing, J. Zhao, P.S. Conti, K. Chen, Radiolabeled nanoparticles for multimodality tumor imaging, Theranostics. 4 (2014) 290–306, https://doi.org/10.7150/thno.7341.

[42] F.-M. Lu, Z. Yuan, PET/SPECT molecular imaging in clinical neuroscience: recent advances in the investigation of CNS diseases, Quant. Imaging Med. Surg. 5 (2015) 433–447, https://doi.org/10.3978/j.issn.2223-4292.2015.03.16.

[43] S. Kalimuthu, J.H. Jeong, J.M. Oh, B.C. Ahn, Drug discovery by molecular imaging and monitoring therapy response in lymphoma, Int. J. Mol. Sci. 18 (2017) 1639, https://doi.org/10.3390/ijms18081639.

[44] K. Heinzmann, L.M. Carter, J.S. Lewis, E.O. Aboagye, Multiplexed imaging for diagnosis and therapy, Nat. Biomed. Eng. 1 (2017) 697–713, https://doi.org/10.1038/s41551-017-0131-8.

[45] J. Weber, U. Haberkorn, W. Mier, Cancer stratification by molecular imaging, Int. J. Mol. Sci. 16 (2015) 4918–4946, https://doi.org/10.3390/ijms16034918.

[46] R.M. de Kruijff, H.T. Wolterbeek, A.G. Denkova, A critical review of alpha radionuclide therapy - how to deal with recolining daughters? Pharmaceuticals. 8 (2015) 321–336, https://doi.org/10.3390/ph8020321.

[47] S. Goel, C.G. England, F. Chen, W. Cai, Positron emission tomography and nanotechnology: a dynamic duo for cancer theranostics, Adv. Drug Deliv. Rev. 113 (2017) 157–176, https://doi.org/10.1016/j.addr.2016.08.001.

[48] J. Lamb, J.P. Holland, Advanced methods for Radiolabeling multimodality nanomedicines for SPECT/MRI and PET/MRI, J. Nucl. Med. 59 (2018) 382–389, https://doi.org/10.2967/jnumed.116.187419.

[49] S. Goel, F. Chen, E.B. Ehlerding, W. Cai, Intrinsically radiolabeled nanoparticles: an emerging paradigm, Small. 10 (2014) 3825–3830, https://doi.org/10.1002/smll.201401048.

[50] J. Jeon, Review of therapeutic applications of Radiolabeled functional nanomaterials, Int. J. Mol. Sci. 20 (2019) 2323, https://doi.org/10.3390/ijms20092323.

[51] Y. Liu, M.J. Welch, Nanoparticles labeled with positron emitting nuclides: advantages, methods, and applications, Bioconjug. Chem. 23 (2012) 671–682, https://doi.org/10.1021/bc200264c.

[52] L. Farzin, S. Sheibani, M.E. Moassesi, M. Shamsipur, An overview of nanoscale radionuclides and radiolabeled nanomaterials commonly used for nuclear molecular imaging and therapeutic functions, J. Biomed. Mater. Res. A 107 (2019) 251–285, https://doi.org/10.1002/jbm.a.36550.

[53] Y. Liu, Q. Miao, P. Zou, L. Liu, X. Wang, L. An, X. Zhang, X. Qian, S. Luo, G. Liang, Enzyme-controlled intracellular self-assembly of (18)F nanoparticles for enhanced MicroPET imaging of tumor, Theranostics. 5 (2015) 1058–1067, https://doi.org/10.7150/thno.11758.

[54] S. Rojas, J.D. Gispert, R. Martín, S. Abad, C. Menchón, D. Pareto, V.M. Víctor, M. Álvaro, H. García, J.R. Herance, Biodistribution of amino-functionalized diamond nanoparticles. In vivo studies based on 18F radionuclide emission, ACS Nano 5 (2011) 5552–5559, https://doi.org/10.1021/nn200986z.

[55] L. Xiong, B. Shen, D. Behera, S.S. Gambhir, F.T. Chin, J. Rao, Synthesis of ligand-functionalized water-soluble [18F]YF3 nanoparticles for PET imaging, Nanoscale. 5 (2013) 3253–3256, https://doi.org/10.1039/C3NR00335C.

[56] P.P. Di Mauro, V. Gómez-Vallejo, Z. Baz Maldonado, J. Llop Roig, S. Borrós, Novel 18F Labeling strategy for polyester-based NPs for in vivo PET-CT imaging, Bioconjug. Chem. 26 (2015) 582–592, https://doi.org/10.1021/acs.bioconjchem.5b00040.

[57] J. Zhu, J. Chin, C. Wängler, B. Wängler, R.B. Lennox, R. Schirrmacher, Rapid 18F-Labeling and loading of PEGylated gold nanoparticles for in vivo applications, Bioconjug. Chem. 25 (2014) 1143–1150, https://doi.org/10.1021/bc5001593.

[58] M. Jauregui-Osoro, P.A. Williamson, A. Glaria, K. Sunassee, P. Charoenphun, M.A. Green, G.E.D. Mullen, P.J. Blower, Biocompatible inorganic nanoparticles for [18F]-fluoride binding with applications in PET imaging, Dalton Trans. 40 (2011) 6226–6237, https://doi.org/10.1039/C0DT01618G.

[59] J. Zhou, M. Yu, Y. Sun, X. Zhang, X. Zhu, Z. Wu, D. Wu, F. Li, Fluorine-18-labeled Gd3+/Yb3+/Er3+ co-doped NaYF4 nanophosphors for multimodality PET/MR/UCL imaging, Biomaterials. 32 (2011) 1148–1156, https://doi.org/10.1016/j.biomaterials.2010.09.071.

[60] Y. Zhao, D. Sultan, L. Detering, S. Cho, G. Sun, R. Pierce, K.L. Wooley, Y. Liu, Copper-64-alloyed gold nanoparticles for cancer imaging: improved radiolabel stability and diagnostic accuracy, Angew. Chem. Int. Ed. 53 (2014) 156–159, https://doi.org/10.1002/anie.201308494.

[61] M. Zhou, R. Zhang, M. Huang, W. Lu, S. Song, M.P. Melancon, M. Tian, D. Liang, C. Li, A Chelator-free multifunctional [64Cu]CuS nanoparticle platform for simultaneous micro-PET/CT imaging and Photothermal ablation therapy, J. Am. Chem. Soc. 132 (2010) 15351–15358, https://doi.org/10.1021/ja106855m.

[62] B.R. Jarrett, B. Gustafsson, D.L. Kukis, A.Y. Louie, Synthesis of 64Cu-Labeled magnetic nanoparticles for multimodal imaging, Bioconjug. Chem. 19 (2008) 1496–1504, https://doi.org/10.1021/bc800108v.

[63] E. Andreozzi, J.W. Seo, K. Ferrara, A. Louie, Novel method to label solid lipid nanoparticles with 64Cu for positron emission tomography imaging, Bioconjug. Chem. 22 (2011) 808–818, https://doi.org/10.1021/bc100478k.

[64] T.W. Liu, T.D. MacDonald, J. Shi, B.C. Wilson, G. Zheng, Intrinsically Copper-64-Labeled organic nanoparticles as radiotracers, Angew. Chem. Int. Ed. 51 (2012) 13128–13131, https://doi.org/10.1002/anie.201206939.

[65] D. Jiang, Z. Ge, H.-J. Im, C.G. England, D. Ni, J. Hou, L. Zhang, C.J. Kutyreff, Y. Yan, Y. Liu, S.Y. Cho, J.W. Engle, J. Shi, P. Huang, C. Fan, H. Yan, W. Cai, DNA origami nanostructures can exhibit preferential renal uptake and alleviate acute kidney injury, Nat. Biomed. Eng. 2 (2018) 865–877, https://doi.org/10.1038/s41551-018-0317-8.

[66] E.D. Pressly, R. Rossin, A. Hagooly, K. Fukukawa, B.W. Messmore, M.J. Welch, K.L. Wooley, M.S. Lamm, R.A. Hule, D.J. Pochan, C.J. Hawker, Structural effects on the biodistribution and positron emission tomography (PET) imaging of well-defined 64Cu-Labeled nanoparticles comprised of amphiphilic block graft copolymers, Biomacromolecules. 8 (2007) 3126–3134, https://doi.org/10.1021/bm700541e.

[67] R. Rossin, S. Muro, M.J. Welch, V.R. Muzykantov, D.P. Schuster, In vivo imaging of 64Cu-Labeled polymer nanoparticles targeted to the lung endothelium, J. Nucl. Med. 49 (2008) 103–111, https://doi.org/10.2967/jnumed.107.045302.

[68] D.-E. Lee, J.H. Na, S. Lee, C.M. Kang, H.N. Kim, S.J. Han, H. Kim, Y.S. Choe, K.-H. Jung, K.C. Lee, K. Choi, I.C. Kwon, S.Y. Jeong, K.-H. Lee, K. Kim, Facile method to radiolabel glycol chitosan nanoparticles with 64Cu via copper-free click chemistry for MicroPET imaging, Mol. Pharm. 10 (2013) 2190–2198, https://doi.org/10.1021/mp300601r.

[69] R. Chakravarty, S. Goel, H. Hong, F. Chen, H.F. Valdovinos, R. Hernandez, T.E. Barnhart, W. Cai, Hollow mesoporous silica nanoparticles for tumor vasculature targeting and PET image-guided drug delivery, Nanomedicine. 10 (2015) 1233–1246, https://doi.org/10.2217/nnm.14.226.

[70] F. Gao, P. Cai, W. Yang, J. Xue, L. Gao, R. Liu, Y. Wang, Y. Zhao, X. He, L. Zhao, G. Huang, F. Wu, Y. Zhao, Z. Chai, X. Gao, Ultrasmall [64Cu]cu nanoclusters for targeting Orthotopic lung Tumors using accurate positron emission tomography imaging, ACS Nano 9 (2015) 4976–4986, https://doi.org/10.1021/nn507130k.

[71] J.W. Seo, H. Baek, L.M. Mahakian, J. Kusunose, J. Hamzah, E. Ruoslahti, K.W. Ferrara, 64Cu-Labeled LyP-1-dendrimer for PET-CT imaging of atherosclerotic plaque, Bioconjug. Chem. 25 (2014) 231–239, https://doi.org/10.1021/bc400347s.

[72] X. Sun, X. Huang, J. Guo, W. Zhu, Y. Ding, G. Niu, A. Wang, D.O. Kiesewetter, Z.L. Wang, S. Sun, X. Chen, Self-illuminating 64Cu-doped CdSe/ZnS nanocrystals for in vivo tumor imaging, J. Am. Chem. Soc. 136 (2014) 1706–1709, https://doi.org/10.1021/ja410438n.

[73] Y. Sun, Q. Liu, J. Peng, W. Feng, Y. Zhang, P. Yang, F. Li, Radioisotope post-labeling upconversion nanophosphors for in vivo quantitative tracking, Biomaterials. 34 (2013) 2289–2295, https://doi.org/10.1016/j.biomaterials.2012.11.047.

[74] J. Frigell, I. García, V. Gómez-Vallejo, J. Llop, S. Penadés, 68Ga-Labeled gold Glyconanoparticles for exploring blood–brain barrier permeability: preparation, biodistribution studies, and improved brain uptake via neuropeptide conjugation, J. Am. Chem. Soc. 136 (2014) 449–457, https://doi.org/10.1021/ja411096m.

[75] R. Madru, T.A. Tran, J. Axelsson, C. Ingvar, A. Bibic, F. Ståhlberg, L. Knutsson, S.-E. Strand, (68)Ga-labeled superparamagnetic iron oxide nanoparticles (SPIONs) for multi-modality PET/MR/Cherenkov luminescence imaging of sentinel lymph nodes, Am. J. Nucl. Med. Mol. Imaging. 4 (2014) 60–69.

[76] J. Pellico, J. Ruiz-Cabello, M. Saiz-Alía, G. del Rosario, S. Caja, M. Montoya, L. de Manuel, M.P. Morales, L. Gutiérrez, B. Galiana, J.A. Enríquez, F. Herranz, Fast synthesis and bioconjugation of 68Ga core-doped extremely small iron oxide nanoparticles for PET/MR imaging, Contrast Media Mol. Imaging. 11 (2016) 203–210, https://doi.org/10.1002/cmmi.1681.

[77] C. Truillet, P. Bouziotis, C. Tsoukalas, J. Brugière, M. Martini, L. Sancey, T. Brichart, F. Denat, F. Boschetti, U. Darbost, I. Bonnamour, D. Stellas, C.D. Anagnostopoulos, V. Koutoulidis, L.A. Moulopoulos, P. Perriat, F. Lux, O. Tillement, Ultrasmall particles for Gd-MRI and 68Ga-PET dual imaging, Contrast Media Mol. Imaging. 10 (2015) 309–319, https://doi.org/10.1002/cmmi.1633.

[78] R. Chakravarty, H.F. Valdovinos, F. Chen, C.M. Lewis, P.A. Ellison, H. Luo, M.E. Meyerand, R.J. Nickles, W. Cai, Intrinsically Germanium-69-Labeled Iron oxide nanoparticles: synthesis and in-vivo dual-modality PET/MR imaging, Adv. Mater. 26 (2014) 5119–5123, https://doi.org/10.1002/adma.201401372.

[79] R. Chakravarty, H. Valdovinos, F. Chen, P. Ellison, R. Nickles, W. Cai, Facile synthesis of 69Ge-labeled nanoparticles for dual-modality PET/MRI, J. Nucl. Med. 55 (2014) 1049.

[80] C. Perez-Medina, D. Abdel-Atti, J. Tang, Y. Zhao, Z.A. Fayad, J.S. Lewis, W.J. Mulder, T. Reiner, Nanoreporter PET predicts the efficacy of anti-cancer nanotherapy, Nat. Commun. 7 (2016) 11838, https://doi.org/10.1038/ncomms11838.

[81] M. Lameijer, T. Binderup, M.M.T. van Leent, M.L. Senders, F. Fay, J. Malkus, B.L. Sanchez-Gaytan, A.J.P. Teunissen, N. Karakatsanis, P. Robson, X. Zhou, Y. Ye, G. Wojtkiewicz, J. Tang, T.T.P. Seijkens, J. Kroon, E.S.G. Stroes, A. Kjaer, J. Ochando, T. Reiner, C. Pérez-Medina, C. Calcagno, E.A. Fischer, B. Zhang, R.E. Temel, F.K. Swirski, M. Nahrendorf, Z.A. Fayad, E. Lutgens, W.J.M. Mulder, R. Duivenvoorden, Efficacy and safety assessment of a TRAF6-targeted nanoimmunotherapy in atherosclerotic mice and non-human primates, Nat. Biomed. Eng. 2 (2018) 279–292, https://doi.org/10.1038/s41551-018-0221-2.

[82] D.S. Abou, D.L.J. Thorek, N.N. Ramos, M.W.H. Pinkse, H.T. Wolterbeek, S.D. Carlin, B.J. Beattie, J.S. Lewis, 89Zr-Labeled paramagnetic octreotide-liposomes for PET-MR imaging of cancer, Pharm. Res. 30 (2013) 878–888, https://doi.org/10.1007/s11095-012-0929-8.

[83] F. Ai, S. Goel, Y. Zhan, H.F. Valdovinos, F. Chen, T.E. Barnhart, W. Cai, Intrinsically (89)Zr-labeled Gd(2)O(2)S:Eu nanophosphors with high in vivo stability for dual-modality imaging, Am. J. Transl. Res. 8 (2016) 5591–5600.

[84] C. Truillet, E. Thomas, F. Lux, L.T. Huynh, O. Tillement, M.J. Evans, Synthesis and characterization of 89Zr-Labeled Ultrasmall nanoparticles, Mol. Pharm. 13 (2016) 2596–2601, https://doi.org/10.1021/acs.molpharmaceut.6b00264.

[85] E.J. Keliher, J. Yoo, M. Nahrendorf, J.S. Lewis, B. Marinelli, A. Newton, M.J. Pittet, R. Weissleder, 89Zr-labeled dextran nanoparticles allow in vivo macrophage imaging, Bioconjug. Chem. 22 (2011) 2383–2389, https://doi.org/10.1021/bc200405d.

[86] F. Chen, S. Goel, H.F. Valdovinos, H. Luo, R. Hernandez, T.E. Barnhart, W. Cai, In vivo integrity and biological fate of Chelator-free Zirconium-89-Labeled mesoporous silica nanoparticles, ACS Nano 9 (2015) 7950–7959, https://doi.org/10.1021/acsnano.5b00526.

[87] L. Kramer, G. Winter, B. Baur, A.J. Kuntz, T. Kull, C. Solbach, A.J. Beer, M. Lindén, Quantitative and correlative biodistribution analysis of 89Zr-labeled mesoporous silica nanoparticles intravenously injected into tumor-bearing mice, Nanoscale. 9 (2017) 9743–9753, https://doi.org/10.1039/C7NR02050C.

[88] L.W.E. Starmans, M.A.P.M. Hummelink, R. Rossin, E.C.M. Kneepkens, R. Lamerichs, K. Donato, K. Nicolay, H. Grüll, 89Zr- and Fe-Labeled polymeric micelles for dual

modality PET and T1-weighted MR imaging, Adv. Healthc. Mater. 4 (2015) 2137–2145, https://doi.org/10.1002/adhm.201500414.
[89] A. Ruggiero, C.H. Villa, J.P. Holland, S.R. Sprinkle, C. May, J.S. Lewis, D.A. Scheinberg, M.R. McDevitt, Imaging and treating tumor vasculature with targeted radiolabeled carbon nanotubes, Int. J. Nanomedicine 5 (2010) 783–802, https://doi.org/10.2147/IJN.S13300.
[90] H.B.S. Chan, B.L. Ellis, H.L. Sharma, W. Frost, V. Caps, R.A. Shields, S.C. Tsang, Carbon-encapsulated radioactive 99mTc nanoparticles, Adv. Mater. 16 (2004) 144–149, https://doi.org/10.1002/adma.200305407.
[91] D. Psimadas, P. Bouziotis, P. Georgoulias, V. Valotassiou, T. Tsotakos, G. Loudos, Radiolabeling approaches of nanoparticles with 99mTc, Contrast Media Mol. Imaging. 8 (2013) 333–339, https://doi.org/10.1002/cmmi.1530.
[92] T. Banerjee, S. Mitra, A.K. Singh, R.K. Sharma, A. Maitra, Preparation, characterization and biodistribution of ultrafine chitosan nanoparticles, Int. J. Pharm. 243 (2002) 93–105, https://doi.org/10.1016/S0378-5173(02)00267-3.
[93] D. Jiang, Y. Sun, J. Li, Q. Li, M. Lv, B. Zhu, T. Tian, D. Cheng, J. Xia, L. Zhang, L. Wang, Q. Huang, J. Shi, C. Fan, Multiple-armed tetrahedral DNA nanostructures for tumor-targeting, dual-modality in vivo imaging, ACS Appl. Mater. Interfaces 8 (2016) 4378–4384, https://doi.org/10.1021/acsami.5b10792.
[94] S.-G. Yang, J.-E. Chang, B. Shin, S. Park, K. Na, C.-K. Shim, 99mTc-hematoporphyrin linked albumin nanoparticles for lung cancer targeted photodynamic therapy and imaging, J. Mater. Chem. 20 (2010) 9042–9046, https://doi.org/10.1039/C0JM01544J.
[95] D. Psimadas, P. Georgoulias, V. Valotassiou, G. Loudos, Molecular nanomedicine towards cancer: 111In-Labeled nanoparticles, J. Pharm. Sci. 101 (2012) 2271–2280, https://doi.org/10.1002/jps.23146.
[96] M.M. Tsotsalas, K. Kopka, G. Luppi, S. Wagner, M.P. Law, M. Schäfers, L. De Cola, Encapsulating 111In in nanocontainers for scintigraphic imaging: synthesis, characterization, and in vivo biodistribution, ACS Nano 4 (2010) 342–348, https://doi.org/10.1021/nn901166u.
[97] J. Zeng, B. Jia, R. Qiao, C. Wang, L. Jing, F. Wang, M. Gao, In situ 111In-doping for achieving biocompatible and non-leachable 111In-labeled Fe3O4 nanoparticles, Chem. Commun. 50 (2014) 2170–2172, https://doi.org/10.1039/C3CC48948E.
[98] R.R. Patil, J. Yu, S.R. Banerjee, Y. Ren, D. Leong, X. Jiang, M. Pomper, B. Tsui, D.L. Kraitchman, H.-Q. Mao, Probing in vivo trafficking of polymer/DNA micellar nanoparticles using SPECT/CT imaging, Mol. Ther. 19 (2011) 1626–1635, https://doi.org/10.1038/mt.2011.128.
[99] R. Zhang, C. Xiong, M. Huang, M. Zhou, Q. Huang, X. Wen, D. Liang, C. Li, Peptide-conjugated polymeric micellar nanoparticles for dual SPECT and optical imaging of EphB4 receptors in prostate cancer xenografts, Biomaterials. 32 (2011) 5872–5879, https://doi.org/10.1016/j.biomaterials.2011.04.070.
[100] M.R. McDevitt, D. Chattopadhyay, B.J. Kappel, J.S. Jaggi, S.R. Schiffman, C. Antczak, J.T. Njardarson, R. Brentjens, D.A. Scheinberg, Tumor targeting with antibody-functionalized, Radiolabeled carbon nanotubes, J. Nucl. Med. 48 (2007) 1180–1189, https://doi.org/10.2967/jnumed.106.039131.
[101] S.B. Lee, S.-W. Lee, S.Y. Jeong, G. Yoon, S.J. Cho, S.K. Kim, I.-K. Lee, B.-C. Ahn, J. Lee, Y.H. Jeon, Engineering of radioiodine-Labeled gold Core–Shell nanoparticles as efficient nuclear medicine imaging agents for trafficking of dendritic cells, ACS Appl. Mater. Interfaces 9 (2017) 8480–8489, https://doi.org/10.1021/acsami.6b14800.
[102] E.A. Simone, B.J. Zern, A.-M. Chacko, J.L. Mikitsh, E.R. Blankemeyer, S. Muro, R.V. Stan, V.R. Muzykantov, Endothelial targeting of polymeric nanoparticles stably labeled with the PET imaging radioisotope iodine-124, Biomaterials. 33 (2012) 5406–5413, https://doi.org/10.1016/j.biomaterials.2012.04.036.
[103] G. Engudar, H. Schaarup-Jensen, F.P. Fliedner, A.E. Hansen, P. Kempen, R.I. Jølck, A. Kjær, T.L. Andresen, M.H. Clausen, A.I. Jensen, J.R. Henriksen, Remote loading of liposomes with a (124)I-radioiodinated compound and their in vivo evaluation by PET/CT in a murine tumor model, Theranostics. 8 (2018) 5828–5841, https://doi.org/10.7150/thno.26706.
[104] R. Kumar, I. Roy, T.Y. Ohulchanskky, L. a Vathy, E.J. Bergey, M. Sajjad, P.N. Prasad, In Vivo Biodistribution and Clearance Studies Using Multimodal Organically Modified Silica Nanoparticles, 4, 2010 699–708.
[105] U. Kostiv, V. Lobaz, J. Kučka, P. Švec, O. Sedláček, M. Hrubý, O. Janoušková, P. Francová, V. Kolářová, L. Šefc, D. Horák, A simple neridronate-based surface coating strategy for upconversion nanoparticles: highly colloidally stable 125I-radiolabeled NaYF4:Yb3+/Er3+@PEG nanoparticles for multimodal in vivo tissue imaging, Nanoscale. 9 (2017) 16680–16688, https://doi.org/10.1039/C7NR05456D.
[106] S.-L. Li, T. Xiao, W. Xia, X. Ding, Y. Yu, J. Jiang, L. Wang, New light on the ring-chain equilibrium of a hydrogen-bonded supramolecular polymer based on a photochromic Dithienylethene unit and its energy-transfer properties as a storage material, Chem. Eur. J. 17 (2011) 10716–10723, https://doi.org/10.1002/chem.201100691.
[107] A. Agarwal, X. Shao, J.R. Rajian, H. Zhang, D.L. Chamberland, N.A. Kotov, X. Wang, Dual-mode imaging with radiolabeled gold nanorods, J. Biomed. Opt. 16 (2011) 51307, https://doi.org/10.1117/1.3580277.
[108] L. Tian, Q. Chen, X. Yi, G. Wang, J. Chen, P. Ning, K. Yang, Z. Liu, Radionuclide I-131 Labeled albumin-paclitaxel nanoparticles for synergistic combined chemo-radioisotope therapy of Cancer, Theranostics. 7 (2017) 614–623, https://doi.org/10.7150/thno.17381.
[109] L. Zhao, J. Zhu, Y. Cheng, Z. Xiong, Y. Tang, L. Guo, X. Shi, J. Zhao, Chlorotoxin-conjugated multifunctional dendrimers Labeled with radionuclide 131I for single photon emission computed tomography imaging and radiotherapy of gliomas, ACS Appl. Mater. Interfaces 7 (2015) 19798–19808, https://doi.org/10.1021/acsami.5b05836.
[110] R. He, H. Wang, Y. Su, C. Chen, L. Xie, L. Chen, J. Yu, Y. Toledo, G.S. Abayaweera, G. Zhu, S.H. Bossmann, Incorporating 131I into a PAMAM (G5.0) dendrimer-conjugate: design of a theranostic nanosensor for medullary thyroid carcinoma, RSC Adv. 7 (2017) 16181–16188, https://doi.org/10.1039/C7RA00604G.
[111] L. Chen, X. Zhong, X. Yi, M. Huang, P. Ning, T. Liu, C. Ge, Z. Chai, Z. Liu, K. Yang, Radionuclide 131I labeled reduced graphene oxide for nuclear imaging guided combined radio- and photothermal therapy of cancer, Biomaterials. 66 (2015) 21–28, https://doi.org/10.1016/j.biomaterials.2015.06.043.
[112] Q. Liu, Y. Qian, P. Li, S. Zhang, J. Liu, X. Sun, M. Fulham, D. Feng, G. Huang, W. Lu, S. Song, (131)I-Labeled copper Sulfide-loaded microspheres to treat hepatic tumors via hepatic artery embolization, Theranostics. 8 (2018) 785–799, https://doi.org/10.7150/thno.21491.
[113] Y. Yang, Y. Sun, T. Cao, J. Peng, Y. Liu, Y. Wu, W. Feng, Y. Zhang, F. Li, Hydrothermal synthesis of NaLuF4:153Sm,Yb,Tm nanoparticles and their application in dual-modality upconversion luminescence and SPECT bioimaging, Biomaterials. 34 (2013) 774–783, https://doi.org/10.1016/j.biomaterials.2012.10.022.
[114] J. Peng, Y. Sun, L. Zhao, Y. Wu, W. Feng, Y. Gao, F. Li, Polyphosphoric acid capping radioactive/upconverting NaLuF4:Yb,Tm,153Sm nanoparticles for blood pool imaging in vivo, Biomaterials. 34 (2013) 9535–9544, https://doi.org/10.1016/j.biomaterials.2013.07.098.
[115] Y. Sun, X. Zhu, J. Peng, F. Li, Core–Shell lanthanide upconversion nanophosphors as four-modal probes for tumor angiogenesis imaging, ACS Nano 7 (2013) 11290–11300, https://doi.org/10.1021/nn405082y.
[116] N. Jiménez-Mancilla, G. Ferro-Flores, C. Santos-Cuevas, B. Ocampo-García, M. Luna-Gutiérrez, E. Azorín-Vega, K. Isaac-Olivé, M. Camacho-López, E. Torres-García, Multifunctional targeted therapy system based on 99mTc/177Lu-labeled gold nanoparticles-Tat(49–57)-Lys3-bombesin internalized in nuclei of prostate cancer cells, J. Label. Compd. Radiopharm. 56 (2013) 663–671, https://doi.org/10.1002/jlcr.3087.
[117] S. Yook, Z. Cai, Y. Lu, M.A. Winnik, J.-P. Pignol, R.M. Reilly, Intratumorally injected 177Lu-Labeled gold nanoparticles: gold Nanoseed brachytherapy with application for neoadjuvant treatment of locally advanced breast cancer, J. Nucl. Med. 57 (2016) 936–942, https://doi.org/10.2967/jnumed.115.168906.
[118] A. Gupta, J.H. Shin, M.S. Lee, J.Y. Park, K. Kim, J.H. Kim, M. Suh, C.R. Park, Y.J. Kim, M.G. Song, J.M. Jeong, D.S. Lee, Y.-S. Lee, J.S. Lee, Voxel-based dosimetry of Iron oxide nanoparticle-conjugated 177Lu-Labeled folic acid using SPECT/CT imaging of mice, Mol. Pharm. 16 (2019) 1498–1506, https://doi.org/10.1021/acs.molpharmaceut.8b01125.
[119] B. Yu, H. Wei, Q. He, C.A. Ferreira, C.J. Kutyreff, D. Ni, Z.T. Rosenkrans, L. Cheng, F. Yu, J.W. Engle, X. Lan, W. Cai, Efficient uptake of 177Lu-porphyrin-PEG Nanocomplexes by tumor mitochondria for multimodal-imaging-guided combination therapy, Angew. Chem. Int. Ed. 57 (2018) 218–222, https://doi.org/10.1002/anie.201710232.
[120] A. Soundararajan, G.D. Dodd, A. Bao, W.T. Phillips, L.M. McManus, T.J. Prihoda, B.A. Goins, Chemoradionuclide therapy with 186Re-labeled liposomal doxorubicin in combination with radiofrequency ablation for effective treatment of head and neck Cancer in a nude rat tumor xenograft model, Radiology. 261 (2011) 813–823, https://doi.org/10.1148/radiol.11110361.
[121] A. Soundararajan, A. Bao, W.T. Phillips, R. Perez, B.A. Goins, [186Re]liposomal doxorubicin (Doxil): in vitro stability, pharmacokinetics, imaging and biodistribution in a head and neck squamous cell carcinoma xenograft model, Nucl. Med. Biol. 36 (2009) 515–524, https://doi.org/10.1016/j.nucmedbio.2009.02.004.
[122] S.X. Wang, A. Bao, S.J. Herrera, W.T. Phillips, B. Goins, C. Santoyo, F.R. Miller, R.A. Otto, Intraoperative 186Re-liposome radionuclide therapy in a head and neck squamous cell carcinoma xenograft positive surgical margin model, Clin. Cancer Res. 14 (2008) 3975–3983, https://doi.org/10.1158/1078-0432.CCR-07-4149.
[123] L.-C. Chen, C.-H. Chang, C.-Y. Yu, Y.-J. Chang, Y.-H. Wu, W.-C. Lee, C.-H. Yeh, T.-W. Lee, G. Ting, Pharmacokinetics, micro-SPECT/CT imaging and therapeutic efficacy of 188Re-DXR-liposome in C26 colon carcinoma ascites mice model, Nucl. Med. Biol. 35 (2008) 883–893, https://doi.org/10.1016/j.nucmedbio.2008.09.005.
[124] L.-C. Chen, C.-H. Chang, C.-Y. Yu, Y.-J. Chang, W.-C. Hsu, C.-L. Ho, C.-H. Yeh, T.-Y. Luo, T.-W. Lee, G. Ting, Biodistribution, pharmacokinetics and imaging of 188Re-BMEDA-labeled pegylated liposomes after intraperitoneal injection in a C26 colon carcinoma ascites mouse model, Nucl. Med. Biol. 34 (2007) 415–423, https://doi.org/10.1016/j.nucmedbio.2007.02.003.
[125] Y.-J. Chang, C.-H. Chang, C.-Y. Yu, T.-J. Chang, L.-C. Chen, M.-H. Chen, T.-W. Lee, G. Ting, Therapeutic efficacy and microSPECT/CT imaging of 188Re-DXR-liposome in a C26 murine colon carcinoma solid tumor model, Nucl. Med. Biol. 37 (2010) 95–104, https://doi.org/10.1016/j.nucmedbio.2009.08.006.
[126] J. Lipka, M. Semmler-Behnke, R.A. Sperling, A. Wenk, S. Takenaka, C. Schleh, T. Kissel, W.J. Parak, W.G. Kreyling, Biodistribution of PEG-modified gold nanoparticles following intratracheal instillation and intravenous injection, Biomaterials. 31 (2010) 6574–6581, https://doi.org/10.1016/j.biomaterials.2010.05.009.
[127] Y. Wang, Y. Liu, H. Luehmann, X. Xia, D. Wan, C. Cutler, Y. Xia, Radioluminescent gold nanocages with controlled radioactivity for real-time in vivo imaging, Nano Lett. 13 (2013) 581–585, https://doi.org/10.1021/nl304111v.
[128] K.C.L. Black, Y. Wang, H.P. Luehmann, X. Cai, W. Xing, B. Pang, Y. Zhao, C.S. Cutler, L.V. Wang, Y. Liu, Y. Xia, Radioactive 198Au-doped nanostructures with different shapes for in vivo analyses of their biodistribution, tumor uptake, and Intratumoral distribution, ACS Nano 8 (2014) 4385–4394, https://doi.org/10.1021/nn406258m.
[129] S. Sofou, B.J. Kappel, J.S. Jaggi, M.R. McDevitt, D.A. Scheinberg, G. Sgouros, Enhanced retention of the α-particle-emitting daughters of Actinium-225 by liposome carriers, Bioconjug. Chem. 18 (2007) 2061–2067, https://doi.org/10.1021/bc070075t.
[130] G. Sgouros, S. Sofou, J.L. Thomas, M.R. McDevitt, D.A. Scheinberg, Liposomal encapsulation of 225Ac for targeted nanogenerator therapy of cancer, Cancer Res. 64 (2004) 956–957.
[131] R.M. de Kruijff, K. Drost, L. Thijssen, A. Morgenstern, F. Bruchertseifer, D. Lathouwers, H.T. Wolterbeek, A.G. Denkova, Improved 225Ac daughter retention

in InPO4 containing polymersomes, Appl. Radiat. Isot. 128 (2017) 183–189, https://doi.org/10.1016/j.apradiso.2017.07.030.
[132] R.M. de Kruijff, R. Raavé, A. Kip, J. Molkenboer-Kuenen, A. Morgenstern, F. Bruchertseifer, S. Heskamp, A.G. Denkova, The in vivo fate of (225)Ac daughter nuclides using polymersomes as a model carrier, Sci. Rep. 9 (2019) 11671, https://doi.org/10.1038/s41598-019-48298-8.
[133] J. Woodward, S.J. Kennel, A. Stuckey, D. Osborne, J. Wall, A.J. Rondinone, R.F. Standaert, S. Mirzadeh, LaPO4 nanoparticles doped with Actinium-225 that partially sequester daughter radionuclides, Bioconjug. Chem. 22 (2011) 766–776, https://doi.org/10.1021/bc100574f.
[134] R. Chakravarty, S. Chakraborty, A. Guleria, A. Kunwar, H.D. Sarma, A. Dash, Facile one-pot synthesis of intrinsically Radiolabeled 64Cu-human serum albumin nanocomposite for Cancer targeting, ChemistrySelect. 2 (2017) 8043–8051, https://doi.org/10.1002/slct.201701237.
[135] H. Gupta, M. Aqil, R.K. Khar, A. Ali, A. Bhatnagar, G. Mittal, Sparfloxacin-loaded PLGA nanoparticles for sustained ocular drug delivery, Nanomed. Nanotechnol. Biol. Med. 6 (2010) 324–333, https://doi.org/10.1016/j.nano.2009.10.004.
[136] R. Littich, P.J.H. Scott, Novel strategies for Fluorine-18 radiochemistry, Angew. Chem. Int. Ed. 51 (2012) 1106–1109, https://doi.org/10.1002/anie.201106785.
[137] R.M. Wong, D.A. Gilbert, K. Liu, A.Y. Louie, Rapid size-controlled synthesis of dextran-coated, 64Cu-doped Iron oxide nanoparticles, ACS Nano 6 (2012) 3461–3467, https://doi.org/10.1021/nn300494k.
[138] T. Paik, A.-M. Chacko, J.L. Mikitsh, J.S. Friedberg, D.A. Pryma, C.B. Murray, Shape-controlled synthesis of isotopic Yttrium-90-Labeled rare earth fluoride nanocrystals for multimodal imaging, ACS Nano 9 (2015) 8718–8728, https://doi.org/10.1021/acsnano.5b03355.
[139] W.T. Phillips, B.A. Goins, A. Bao, Radioactive liposomes, Wiley Interdiscip. Rev. Nanomed. Nanobiotechnol. 1 (2009) 69–83, https://doi.org/10.1002/wnan.3.
[140] B.T. Cisneros, J.J. Law, M.L. Matson, A. Azhdarinia, E.M. Sevick-Muraca, L.J. Wilson, Stable confinement of positron emission tomography and magnetic resonance agents within carbon nanotubes for bimodal imaging, Nanomedicine (London) 9 (2014) 2499–2509, https://doi.org/10.2217/nnm.14.26.
[141] D.H. Son, S.M. Hughes, Y. Yin, A. Paul Alivisatos, Cation exchange reactions in ionic nanocrystals, Science. 306 (2004) 1009–1012, https://doi.org/10.1126/science.1103755.
[142] B.J. Beberwyck, Y. Surendranath, A.P. Alivisatos, Cation exchange: a versatile tool for nanomaterials synthesis, J. Phys. Chem. C 117 (2013) 19759–19770, https://doi.org/10.1021/jp405989z.
[143] T. Ruth, Accelerating production of medical isotopes, Nature. 457 (2009) 536–537, https://doi.org/10.1038/457536a.
[144] W.C.W. Chan, D.J. Maxwell, X. Gao, R.E. Bailey, M. Han, S. Nie, Luminescent quantum dots for multiplexed biological detection and imaging, Curr. Opin. Biotechnol. 13 (2002) 40–46, https://doi.org/10.1016/S0958-1669(02)00282-3.
[145] I.L. Medintz, A.R. Clapp, H. Mattoussi, E.R. Goldman, B. Fisher, J.M. Mauro, Self-assembled nanoscale biosensors based on quantum dot FRET donors, Nat. Mater. 2 (2003) 630–638, https://doi.org/10.1038/nmat961.
[146] M.-K. So, C. Xu, A.M. Loening, S.S. Gambhir, J. Rao, Self-illuminating quantum dot conjugates for in vivo imaging, Nat. Biotechnol. 24 (2006) 339–343, https://doi.org/10.1038/nbt1188.
[147] F. Wang, Y. Han, C.S. Lim, Y. Lu, J. Wang, J. Xu, H. Chen, C. Zhang, M. Hong, X. Liu, Simultaneous phase and size control of upconversion nanocrystals through lanthanide doping, Nature. 463 (2010) 1061–1065, https://doi.org/10.1038/nature08777.
[148] A. Chrastina, J.E. Schnitzer, Iodine-125 radiolabeling of silver nanoparticles for in vivo SPECT imaging, Int. J. Nanomedicine 5 (2010) 653–659, https://doi.org/10.2147/IJN.S11677.
[149] S. Guerrero, J.R. Herance, S. Rojas, J.F. Mena, J.D. Gispert, G.A. Acosta, F. Albericio, M.J. Kogan, Synthesis and in vivo evaluation of the biodistribution of a 18F-Labeled conjugate gold-nanoparticle-peptide with potential biomedical application, Bioconjug. Chem. 23 (2012) 399–408, https://doi.org/10.1021/bc200362a.
[150] N.K. Devaraj, E.J. Keliher, G.M. Thurber, M. Nahrendorf, R. Weissleder, 18F labeled nanoparticles for in vivo PET-CT imaging, Bioconjug. Chem. 20 (2009) 397–401, https://doi.org/10.1021/bc8004649.
[151] S. Yook, Y. Lu, J.J. Jeong, Z. Cai, L. Tong, R. Alwarda, J.-P. Pignol, M.A. Winnik, R.M. Reilly, Stability and biodistribution of thiol-functionalized and 177Lu-Labeled metal chelating polymers bound to gold nanoparticles, Biomacromolecules. 17 (2016) 1292–1302, https://doi.org/10.1021/acs.biomac.5b01642.
[152] Y. Zhao, T.M. Shaffer, S. Das, C. Pérez-Medina, W.J.M. Mulder, J. Grimm, Near-infrared quantum dot and 89Zr dual-Labeled nanoparticles for in vivo Cerenkov imaging, Bioconjug. Chem. 28 (2017) 600–608, https://doi.org/10.1021/acs.bioconjchem.6b00687.
[153] T. Binderup, R. Duivenvoorden, F. Fay, M.M.T. van Leent, J. Malkus, S. Baxter, S. Ishino, Y. Zhao, B. Sanchez-Gaytan, A.J.P. Teunissen, Y.C.A. Frederico, J. Tang, G. Carlucci, S. Lyashchenko, C. Calcagno, N. Karakatsanis, G. Soultanidis, M.L. Senders, P.M. Robson, V. Mani, S. Ramachandran, M.E. Lobatto, B.A. Hutten, J.F. Granada, T. Reiner, F.K. Swirski, M. Nahrendorf, A. Kjaer, E.A. Fisher, Z.A. Fayad, C. Pérez-Medina, W.J.M. Mulder, Imaging-assisted nanoimmunotherapy for atherosclerosis in multiple species, Sci. Transl. Med. 11 (2019) eaaw7736, https://doi.org/10.1126/scitranslmed.aaw7736.
[154] A.J. Di Pasqua, H. Yuan, Y. Chung, J.-K. Kim, J.E. Huckle, C. Li, M. Sadgrove, T.H. Tran, M. Jay, X. Lu, Neutron-Activatable holmium-containing mesoporous silica nanoparticles as a potential radionuclide therapeutic agent for ovarian Cancer, J. Nucl. Med. 54 (2013) 111–116, https://doi.org/10.2967/jnumed.112.106609.
[155] I. Munaweera, Y. Shi, B. Koneru, R. Saez, A. Aliev, A.J. Di Pasqua, K.J. Balkus, Chemoradiotherapeutic magnetic nanoparticles for targeted treatment of nonsmall cell lung Cancer, Mol. Pharm. 12 (2015) 3588–3596, https://doi.org/10.1021/acs.molpharmaceut.5b00304.
[156] C. Pérez-Campaña, V. Gómez-Vallejo, M. Puigivila, A. Martín, T. Calvo-Fernández, S.E. Moya, R.F. Ziolo, T. Reese, J. Llop, Biodistribution of different sized nanoparticles assessed by positron emission tomography: a general strategy for direct activation of metal oxide particles, ACS Nano 7 (2013) 3498–3505, https://doi.org/10.1021/nn400450p.
[157] C. Pérez-Campaña, V. Gómez-Vallejo, A. Martin, E. San Sebastián, S.E. Moya, T. Reese, R.F. Ziolo, J. Llop, Tracing nanoparticles in vivo: a new general synthesis of positron emitting metal oxide nanoparticles by proton beam activation, Analyst. 137 (2012) 4902–4906, https://doi.org/10.1039/C2AN35863H.
[158] C. Pérez-Campaña, F. Sansaloni, V. Gómez-Vallejo, Z. Baz, A. Martin, S.E. Moya, J.I. Lagares, R.F. Ziolo, J. Llop, Production of 18F-Labeled titanium dioxide nanoparticles by proton irradiation for biodistribution and biological fate studies in rats, Part. Part. Syst. Charact. 31 (2014) 134–142, https://doi.org/10.1002/ppsc.201300302.
[159] A. Alaarg, M.L. Senders, A. Varela-Moreira, C. Pérez-Medina, Y. Zhao, J. Tang, F. Fay, T. Reiner, Z.A. Fayad, W.E. Hennink, J.M. Metselaar, W.J.M. Mulder, G. Storm, A systematic comparison of clinically viable nanomedicines targeting HMG-CoA reductase in inflammatory atherosclerosis, J. Control. Release 262 (2017) 47–57, https://doi.org/10.1016/j.jconrel.2017.07.013.
[160] C. Pérez-Medina, D. Abdel-Atti, Y. Zhang, V. a Longo, C.P. Irwin, T. Binderup, J. Ruiz-Cabello, Z. a Fayad, J.S. Lewis, W.J.M. Mulder, T. Reiner, A modular Labeling strategy for in vivo PET and near-infrared fluorescence imaging of nanoparticle tumor targeting, J. Nucl. Med. 55 (2014) 1706–1712, https://doi.org/10.2967/jnumed.114.141861.
[161] W.J.M. Mulder, M.M.T. Van Leent, M. Lameijer, E.A. Fisher, Z.A. Fayad, C. Pérez-Medina, High-density lipoprotein nanobiologics for precision medicine, Acc. Chem. Res. 51 (2018) 127–137, https://doi.org/10.1021/acs.accounts.7b00339.
[162] R. Duivenvoorden, J. Tang, D.P. Cormode, A.J. Mieszawska, D. Izquierdo-Garcia, C. Ozcan, M.J. Otten, N. Zaidi, M.E. Lobatto, S.M. van Rijs, B. Priem, E.L. Kuan, C. Martel, B. Hewing, H. Sager, M. Nahrendorf, G.J. Randolph, E.S.G. Stroes, V. Fuster, E. a Fisher, Z. a Fayad, W.J.M. Mulder, A statin-loaded reconstituted high-density lipoprotein nanoparticle inhibits atherosclerotic plaque inflammation, Nat. Commun. 5 (2014) 3065, https://doi.org/10.1038/ncomms4065.
[163] J. Tang, M.E. Lobatto, L. Hassing, S. Van Der Staay, S.M. Van Rijs, C. Calcagno, M.S. Braza, S. Baxter, F. Fay, B.L. Sanchez-Gaytan, R. Duivenvoorden, H.B. Sager, Y.M. Astudillo, W. Leong, S. Ramachandran, G. Storm, C. Pérez-Medina, T. Reiner, D.P. Cormode, G.J. Strijkers, E.S.G. Stroes, F.K. Swirski, M. Nahrendorf, E.A. Fisher, Z.A. Fayad, W.J.M. Mulder, Inhibiting macrophage proliferation suppresses atherosclerotic plaque inflammation, Sci. Adv. 1 (2015) https://doi.org/10.1126/sciadv.1400223.
[164] M.S. Braza, M.M.T.T. van Leent, M. Lameijer, B.L. Sanchez-Gaytan, R.J.W.W. Arts, C. Perez-Medina, P. Conde, M.R. Garcia, M. Gonzalez-Perez, M. Brahmachary, F. Fay, E. Kluza, S. Kossatz, R.J. Dress, F. Salem, A. Rialdi, T. Reiner, P. Boros, G.J. Strijkers, C.C. Calcagno, F. Ginhoux, I. Marazzi, E. Lutgens, G.A.F.F. Nicolaes, C. Weber, F.K. Swirski, M. Nahrendorf, E.A. Fisher, R. Duivenvoorden, Z.A. Fayad, M.G. Netea, W.J.M.M. Mulder, J. Ochando, C. Pérez-Medina, P. Conde, M.R. Garcia, M. Gonzalez-Perez, M. Brahmachary, F. Fay, E. Kluza, S. Kossatz, R.J. Dress, F. Salem, A. Rialdi, T. Reiner, P. Boros, G.J. Strijkers, C.C. Calcagno, F. Ginhoux, I. Marazzi, E. Lutgens, G.A.F.F. Nicolaes, C. Weber, F.K. Swirski, M. Nahrendorf, E.A. Fisher, R. Duivenvoorden, Z.A. Fayad, M.G. Netea, W.J.M.M. Mulder, J. Ochando, Inhibiting inflammation with myeloid cell-specific nanobiologics promotes organ transplant acceptance, Immunity. 49 (2018) 819–828, https://doi.org/10.1016/j.immuni.2018.09.008.
[165] C. Pérez-Medina, T. Binderup, M.E. Lobatto, J. Tang, C. Calcagno, L. Giesen, C.H. Wessel, J. Witjes, S. Ishino, S. Baxter, Y. Zhao, S. Ramachandran, M. Eldib, B.L. Sánchez-Gaytán, P.M. Robson, J. Bini, J.F. Granada, K.M. Fish, E.S.G. Stroes, R. Duivenvoorden, S. Tsimikas, J.S. Lewis, T. Reiner, V. Fuster, A. Kjær, E.A. Fisher, Z.A. Fayad, W.J.M. Mulder, In vivo PET imaging of HDL in multiple atherosclerosis models, JACC Cardiovasc. Imaging 9 (2016) https://doi.org/10.1016/j.jcmg.2016.01.020.
[166] C. Perez-Medina, J. Tang, D. Abdel-Atti, B. Hogstad, M. Merad, E.A. Fisher, Z.A. Fayad, J.S. Lewis, W.J.M. Mulder, T. Reiner, PET imaging of tumor-associated macrophages with 89Zr-labeled HDL nanoparticles, J. Nucl. Med. (2015) 1272–1277, https://doi.org/10.2967/jnumed.115.158956.
[167] J. Tang, S. Baxter, A. Menon, A. Alaarg, B.L. Sanchez-Gaytan, F. Fay, Y. Zhao, M. Ouimet, M.S. Braza, V.A. Longo, D. Abdel-Atti, R. Duivenvoorden, C. Calcagno, G. Storm, S. Tsimikas, K.J. Moore, F.K. Swirski, M. Nahrendorf, E.A. Fisher, C. Pérez-Medina, Z.A. Fayad, T. Reiner, W.J.M. Mulder, Immune cell screening of a nanoparticle library improves atherosclerosis therapy, Proc. Natl. Acad. Sci. 113 (2016) E6731–E6740, https://doi.org/10.1073/pnas.1609629113.
[168] D.W. Bartlett, H. Su, I.J. Hildebrandt, W.A. Weber, M.E. Davis, Impact of tumor-specific targeting on the biodistribution and efficacy of siRNA nanoparticles measured by multimodality in vivo imaging, Proc. Natl. Acad. Sci. U. S. A. 104 (2007) 15549–15554, https://doi.org/10.1073/pnas.0707461104.
[169] O.M. Merkel, D. Librizzi, A. Pfestroff, T. Schurrat, M. Béhé, T. Kissel, In vivo SPECT and real-time gamma camera imaging of biodistribution and pharmacokinetics of siRNA delivery using an optimized radiolabeling and purification procedure, Bioconjug. Chem. 20 (2009) 174–182, https://doi.org/10.1021/bc800408g.
[170] K. Hatanaka, T. Asai, H. Koide, E. Kenjo, T. Tsuzuku, N. Harada, H. Tsukada, N. Oku, Development of double-stranded siRNA labeling method using positron emitter and its in vivo trafficking analyzed by positron emission tomography, Bioconjug. Chem. 21 (2010) 756–763, https://doi.org/10.1021/bc9005267.
[171] E. Koziolová, S. Goel, P. Chytil, O. Janoušková, T.E. Barnhart, W. Cai, T. Etrych, A tumor-targeted polymer theranostics platform for positron emission tomography and fluorescence imaging, Nanoscale. 9 (2017) 10906–10918, https://doi.org/10.1039/C7NR03306K.

[172] L. Jennings, O. Ivashchenko, I.J.C. Marsman, A.C. Laan, A.G. Denkova, G. Waton, F.J. Beekman, F. Schosseler, E. Mendes, In vivo biodistribution of stable spherical and filamentous micelles probed by high-sensitivity SPECT, Biomater. Sci. 4 (2016) 1202–1211, https://doi.org/10.1039/C6BM00297H.

[173] P.R. McDonagh, G. Sundaresan, L. Yang, M. Sun, R. Mikkelsen, J. Zweit, Biodistribution and PET imaging of 89-zirconium labeled cerium oxide nanoparticles synthesized with several surface coatings, Nanomed. Nanotechnol. Biol. Med. 14 (2018) 1429–1440, https://doi.org/10.1016/J.NANO.2018.04.002.

[174] X. Yang, H. Hong, J.J. Grailer, I.J. Rowland, A. Javadi, S.A. Hurley, Y. Xiao, Y. Yang, Y. Zhang, R.J. Nickles, W. Cai, D.A. Steeber, S. Gong, cRGD-functionalized, DOX-conjugated, and ^{64}Cu-labeled superparamagnetic iron oxide nanoparticles for targeted anticancer drug delivery and PET/MR imaging, Biomaterials. 32 (2011) 4151–4160, https://doi.org/10.1016/j.biomaterials.2011.02.006.

[175] A.E. Hansen, A.L. Petersen, J.R. Henriksen, B. Boerresen, P. Rasmussen, D.R. Elema, P.M. af Rosenschöld, A.T. Kristensen, A. Kjær, T.L. Andresen, Positron emission tomography based elucidation of the enhanced permeability and retention effect in dogs with cancer using Copper-64 liposomes, ACS Nano 9 (2015) 6985–6995, https://doi.org/10.1021/acsnano.5b01324.

[176] A.L. Petersen, J.R. Henriksen, T. Binderup, D.R. Elema, P.H. Rasmussen, A.M. Hag, A. Kjær, T.L. Andresen, In vivo evaluation of PEGylated 64Cu-liposomes with theranostic and radiotherapeutic potential using micro PET/CT, Eur. J. Nucl. Med. Mol. Imaging 43 (2016) 941–952, https://doi.org/10.1007/s00259-015-3272-6.

[177] L.W. Locke, M.W. Mayo, A.D. Yoo, M.B. Williams, S.S. Berr, PET imaging of tumor associated macrophages using mannose coated 64Cu liposomes, Biomaterials. 33 (2012) 7785–7793, https://doi.org/10.1016/j.biomaterials.2012.07.022.

[178] F. Zhang, Q. Ni, O. Jacobson, S. Cheng, A. Liao, Z. Wang, Z. He, G. Yu, J. Song, Y. Ma, G. Niu, L. Zhang, G. Zhu, X. Chen, Polymeric nanoparticles with a glutathione-sensitive heterodimeric multifunctional prodrug for in vivo drug monitoring and synergistic Cancer therapy, Angew. Chem. Int. Ed. 57 (2018) 7066–7070, https://doi.org/10.1002/anie.201801984.

[179] Y. Li, T. Lin, Y. Luo, Q. Liu, W. Xiao, W. Guo, D. Lac, H. Zhang, C. Feng, S. Wachsmann-Hogiu, J.H. Walton, S.R. Cherry, D.J. Rowland, D. Kukis, C. Pan, K.S. Lam, A smart and versatile theranostic nanomedicine platform based on nanoporphyrin, Nat. Commun. 5 (2014) 4712, https://doi.org/10.1038/ncomms5712.

[180] Y. Luo, H. Wu, C. Feng, K. Xiao, X. Yang, Q. Liu, T. Lin, H. Zhang, J.H. Walton, Y. Ajena, Y. Hu, K.S. Lam, Y. Li, "One-pot" fabrication of highly versatile and biocompatible poly(vinyl alcohol)-porphyrin-based nanotheranostics, Theranostics. 7 (2017) 3901–3914, https://doi.org/10.7150/thno.20190.

[181] A.L. Petersen, T. Binderup, R.I. Jølck, P. Rasmussen, J.R. Henriksen, A.K. Pfeifer, A. Kjær, T.L. Andresen, Positron emission tomography evaluation of somatostatin receptor targeted 64Cu-TATE-liposomes in a human neuroendocrine carcinoma mouse model, J. Control. Release 160 (2012) 254–263, https://doi.org/10.1016/J.JCONREL.2011.12.038.

[182] C.-F. Wang, M.P. Sarparanta, E.M. Mäkilä, M.L.K. Hyvönen, P.M. Laakkonen, J.J. Salonen, J.T. Hirvonen, A.J. Airaksinen, H.A. Santos, Multifunctional porous silicon nanoparticles for cancer theranostics, Biomaterials. 48 (2015) 108–118, https://doi.org/10.1016/J.BIOMATERIALS.2015.01.008.

[183] H. Lee, D. Gaddy, M. Ventura, N. Bernards, R. de Souza, D. Kirpotin, T. Wickham, J. Fitzgerald, J. Zheng, B.S. Hendriks, Companion diagnostic ^{64} cu-liposome positron emission tomography enables characterization of drug delivery to tumors and predicts response to cancer nanomedicines, Theranostics. 8 (2018) 2300–2312, https://doi.org/10.7150/thno.21670.

[184] A. Ruiz-de-Angulo, A. Zabaleta, V. Gómez-Vallejo, J. Llop, J.C. Mareque-Rivas, Microdosed lipid-coated ^{67} Ga-magnetite enhances antigen-specific immunity by image tracked delivery of antigen and CpG to lymph nodes, ACS Nano 10 (2016) 1602–1618, https://doi.org/10.1021/acsnano.5b07253.

[185] W. Shi, S.M. Ogbomo, N.K. Wagh, Z. Zhou, Y. Jia, S.K. Brusnahan, J.C. Garrison, The influence of linker length on the properties of cathepsin S cleavable (177)Lu-labeled HPMA copolymers for pancreatic cancer imaging, Biomaterials. 35 (2014) 5760–5770, https://doi.org/10.1016/j.biomaterials.2014.03.056.

[186] B. Buckway, N. Frazier, A.J. Gormley, A. Ray, H. Ghandehari, Gold nanorod-mediated hyperthermia enhances the efficacy of HPMA copolymer-90Y conjugates in treatment of prostate tumors, Nucl. Med. Biol. 41 (2014) 282–289, https://doi.org/10.1016/j.nucmedbio.2013.12.002.

[187] W. Zhu, L. Zhao, Y. Fan, J. Zhao, X. Shi, M. Shen, ^{131} I-Labeled multifunctional Polyphosphazene Nanospheres for SPECT imaging-guided radiotherapy of Tumors, Adv. Healthc. Mater. (2019) 1901299, https://doi.org/10.1002/adhm.201901299.

[188] Y. Cheng, J. Zhu, L. Zhao, Z. Xiong, Y. Tang, C. Liu, L. Guo, W. Qiao, X. Shi, J. Zhao, ^{131} I-labeled multifunctional dendrimers modified with BmK CT for targeted SPECT imaging and radiotherapy of gliomas, Nanomedicine. 11 (2016) 1253–1266, https://doi.org/10.2217/nnm-2016-0001.

[189] S. Moeendarbari, R. Tekade, A. Mulgaonkar, P. Christensen, S. Ramezani, G. Hassan, R. Jiang, O.K. Öz, Y. Hao, X. Sun, Theranostic Nanoseeds for efficacious internal radiation therapy of Unresectable solid Tumors, Sci. Rep. 6 (2016) 20614, https://doi.org/10.1038/srep20614.

[190] N. Lamichhane, G.K. Dewkar, G. Sundaresan, R.N. Mahon, J. Zweit, [18F]-fluorinated carboplatin and [111In]-liposome for image-guided drug delivery, Int. J. Mol. Sci. 18 (2017) 1079, https://doi.org/10.3390/ijms18051079.

[191] F. Man, T. Lammers, R. T M de Rosales, Imaging nanomedicine-based drug delivery: a review of clinical studies, Mol. Imaging Biol. 20 (2018) 683–695, https://doi.org/10.1007/s11307-018-1255-2.

[192] M.S. Judenhofer, H.F. Wehrl, D.F. Newport, C. Catana, S.B. Siegel, M. Becker, A. Thielscher, M. Kneilling, M.P. Lichy, M. Eichner, K. Klingel, G. Reischl, S. Widmaier, M. Röcken, R.E. Nutt, H.J. Machulla, K. Uludag, S.R. Cherry, C.D. Claussen, B.J. Pichler, Simultaneous PET-MRI: a new approach for functional and morphological imaging, Nat. Med. 14 (2008) 459–465, https://doi.org/10.1038/nm1700.

[193] S. Kunjachan, J. Ehling, G. Storm, F. Kiessling, T. Lammers, Noninvasive imaging of nanomedicines and Nanotheranostics: principles, Progress, and prospects, Chem. Rev. 115 (2015) 10907–10937, https://doi.org/10.1021/cr500314d.

[194] D. Ni, E.B. Ehlerding, W. Cai, Multimodality imaging agents with PET as the fundamental pillar, Angew. Chem. Int. Ed. 58 (2019) 2570–2579, https://doi.org/10.1002/anie.201806853.

[195] R. Van der Meel, T. Lammers, W.E. Hennink, Cancer nanomedicines: oversold or underappreciated? Expert Opin. Drug Deliv. 14 (2017) 1–5, https://doi.org/10.1080/17425247.2017.1262346.

[196] J.M. Metselaar, T. Lammers, Challenges in nanomedicine clinical translation, Drug Deliv. Transl. Res. (2020) 1–5, https://doi.org/10.1007/s13346-020-00740-5.

[197] B. Børresen, J.R. Henriksen, G. Clergeaud, J.S. Jørgensen, F. Melander, D.R. Elema, J. Szebeni, S.A. Engelholm, A.T. Kristensen, A. Kjær, T.L. Andresen, A.E. Hansen, Theranostic imaging May vaccinate against the therapeutic benefit of long circulating PEGylated liposomes and change cargo pharmacokinetics, ACS Nano 12 (2018) 11386–11398, https://doi.org/10.1021/acsnano.8b06266.

[198] A.S. Abu Lila, H. Kiwada, T. Ishida, The accelerated blood clearance (ABC) phenomenon: clinical challenge and approaches to manage, J. Control. Release 172 (2013) 38–47, https://doi.org/10.1016/j.jconrel.2013.07.026.

[199] F.M. van der Valk, D.F. van Wijk, M.E. Lobatto, H.J. Verberne, G. Storm, M.C.M. Willems, D.A. Legemate, A.J. Nederveen, C. Calcagno, V. Mani, S. Ramachandran, M.P.M. Paridaans, M.J. Otten, G.M. Dallinga-Thie, Z.A. Fayad, M. Nieuwdorp, D.M. Schulte, J.M. Metselaar, W.J.M. Mulder, E.S. Stroes, Prednisolone-containing liposomes accumulate in human atherosclerotic macrophages upon intravenous administration, Nanomedicine. 11 (2015) 1039–1046, https://doi.org/10.1016/j.nano.2015.02.021.

[200] M.E. Lobatto, T. Binderup, P.M. Robson, L.F.P. Giesen, C. Calcagno, J. Witjes, F. Fay, S. Baxter, C.H. Wessel, M. Eldib, J. Bini, S.D. Carlin, E.S.G. Stroes, G. Storm, A. Kjaer, J.S. Lewis, T. Reiner, Z.A. Fayad, W.J.M. Mulder, C. Pérez-Medina, Multimodal positron emission tomography imaging to quantify uptake of 89Zr-Labeled liposomes in the atherosclerotic Vessel Wall, Bioconjug. Chem. 31 (2020) 360–368, https://doi.org/10.1021/acs.bioconjchem.9b00256.

[201] T.J. Beldman, M.L. Senders, A. Alaarg, C. Pérez-Medina, J. Tang, Y. Zhao, F. Fay, J. Deichmöller, B. Born, E. Desclos, N.N. Van Der Wel, R.A. Hoebe, F. Kohen, E. Kartvelishvily, M. Neeman, T. Reiner, C. Calcagno, Z.A. Fayad, M.P.J. De Winther, E. Lutgens, W.J.M. Mulder, E. Kluza, Hyaluronan nanoparticles selectively target plaque-associated macrophages and improve plaque stability in atherosclerosis, ACS Nano 11 (2017) 5785–5799, https://doi.org/10.1021/acsnano.7b01385.

[202] G.H. Petersen, S.K. Alzghari, W. Chee, S.S. Sankari, N.M. La-Beck, Meta-analysis of clinical and preclinical studies comparing the anticancer efficacy of liposomal versus conventional non-liposomal doxorubicin, J. Control. Release 232 (2016) 255–264, https://doi.org/10.1016/j.jconrel.2016.04.028.

[203] G. Lopez-Berestein, L. Kasi, M.G. Rosenblum, T. Haynie, M. Jahns, H. Glenn, R. Mehta, G.M. Mavligit, E.M. Hersh, Clinical pharmacology of 99mTc-labeled liposomes in patients with cancer, Cancer Res. 44 (1984) 375–378.

[204] A.F. Turner, C.A. Presant, R.T. Proffitt, L.E. Williams, D.W. Winsor, J.L. Werner, In-111-labeled liposomes: dosimetry and tumor depiction, Radiology. 166 (1988) 761–765, https://doi.org/10.1148/radiology.166.3.3340774.

[205] C.A. Presant, R.T. Proffitt, A.F. Turner, L.E. Williams, D. Winsor, J.L. Werner, P. Kennedy, C. Wiseman, K. Gala, R.J. McKenna, J.D. Smith, S.A. Bouzaglou, R.A. Callahan, J. Baldeschwieler, R.J. Crossley, Successful imaging of human cancer with indium-111-labeled phospholipid vesicles, Cancer. 62 (1988) 905–911, https://doi.org/10.1002/1097-0142(19880901)62:5<905::AID-CNCR2820620509>3.0.CO;2-3.

[206] S. Stewart, K.J. Harrington, The Biodistribution and Pharmacokinetics of Stealth Liposomes in Patients with Solid Tumors, Oncology 11 (1997) 33–37.

[207] K.J. Harrington, S. Mohammadtaghi, P.S. Uster, D. Glass, A.M. Peters, R.G. Vile, J.S. Stewart, Effective targeting of solid tumors in patients with locally advanced cancers by radiolabeled pegylated liposomes, Clin. Cancer Res. 7 (2001) 243–254.

[208] M.I. Koukourakis, S. Koukouraki, A. Giatromanolaki, S.C. Archimandritis, J. Skarlatos, K. Beroukas, J.G. Bizakis, G. Retalis, N. Karkavitsas, E.S. Helidonis, Liposomal doxorubicin and conventionally fractionated radiotherapy in the treatment of locally advanced non-small-cell lung cancer and head and neck cancer, Acta Oncol. (Madr). 17 (1999) 3512–3521.

[209] M.I. Koukourakis, S. Koukouraki, A. Giatromanolaki, S. Kakolyris, V. Georgoulias, A. Velidaki, S. Archimandritis, N.N. Karkavitsas, High intratumoral accumulation of stealth liposomal doxorubicin in sarcomas - rationale for combination with radiotherapy, Acta Oncol. (Madr). 39 (2000) 207–211, https://doi.org/10.1080/028418600430789.

[210] M.M. Kleiter, D. Yu, L.A. Mohammadian, N. Niehaus, I. Spasojevic, L. Sanders, B.L. Viglianti, P.S. Yarmolenko, M. Hauck, N.A. Petry, T.Z. Wong, M.W. Dewhirst, D.E. Thrall, A tracer dose of technetium-99m- labeled liposomes can estimate the effect of hyperthermia on intratumoral doxil extravasation, Clin. Cancer Res. 12 (2006) 6800–6807, https://doi.org/10.1158/1078-0432.CCR-06-0839.

[211] H. Lee, A.F. Shields, B.A. Siegel, K.D. Miller, I. Krop, C.X. Ma, P.M. LoRusso, P.N. Munster, K. Campbell, D.F. Gaddy, S.C. Leonard, E. Geretti, S.J. Blocker, D.B. Kirpotin, V. Moyo, T.J. Wickham, B.S. Hendriks, 64Cu-MM-302 positron emission tomography quantifies variability of enhanced permeability and retention of nanoparticles in relation to treatment response in patients with metastatic breast cancer, Clin. Cancer Res. 23 (2017) 4190–4202, https://doi.org/10.1158/1078-0432.CCR-16-3193.

[212] P. Munster, I.E. Krop, P. LoRusso, C. Ma, B.A. Siegel, A.F. Shields, I. Molnár, T.J. Wickham, J. Reynolds, K. Campbell, B.S. Hendriks, B.S. Adiwijaya, E. Geretti, V. Moyo, K.D. Miller, Safety and pharmacokinetics of MM-302, a HER2-targeted

antibody–liposomal doxorubicin conjugate, in patients with advanced HER2-positive breast cancer: a phase 1 dose-escalation study, Br. J. Cancer 119 (2018) 1086–1093, https://doi.org/10.1038/s41416-018-0235-2.

[213] H. Giovinazzo, P. Kumar, A. Sheikh, K.M. Brooks, M. Ivanovic, M. Walsh, W.P. Caron, R.J. Kowalsky, G. Song, A. Whitlow, D.L. Clarke-Pearson, W.R. Brewster, L. Van Le, B.A. Zamboni, V. Bae-Jump, P.A. Gehrig, W.C. Zamboni, Technetium Tc 99m sulfur colloid phenotypic probe for the pharmacokinetics and pharmacodynamics of PEGylated liposomal doxorubicin in women with ovarian cancer, Cancer Chemother. Pharmacol. 77 (2016) 565–573, https://doi.org/10.1007/s00280-015-2945-y.

[214] R.K. Ramanathan, R.L. Korn, N. Raghunand, J.C. Sachdev, R.G. Newbold, G. Jameson, G.J. Fetterly, J. Prey, S.G. Klinz, J. Kim, J. Cain, B.S. Hendriks, D.C. Drummond, E. Bayever, J.B. Fitzgerald, Correlation between Ferumoxytol uptake in tumor lesions by MRI and response to Nanoliposomal irinotecan in patients with advanced solid Tumors: a pilot study, Clin. Cancer Res. 23 (2017) 3638–3648, https://doi.org/10.1158/1078-0432.CCR-16-1990.

[215] E. Phillips, O. Penate-medina, P.B. Zanzonico, R.D. Carvajal, P. Mohan, Y. Ye, J. Humm, M. Gönen, H. Kalaigian, H. Schöder, H.W. Strauss, S.M. Larson, U. Wiesner, M.S. Bradbury, Clinical Translation of an Ultrasmall Inorganic Optical-PET Imaging Nanoparticle Probe, 6, 2014 1–10, https://doi.org/10.1126/scitranslmed.3009524.

[216] J.L.J. Dearling, A.B. Packard, Molecular imaging in nanomedicine – a developmental tool and a clinical necessity, J. Control. Release 261 (2017) 23–30, https://doi.org/10.1016/j.jconrel.2017.06.011.

[217] E. Berg, S.R. Cherry, Innovations in instrumentation for positron emission tomography, Semin. Nucl. Med. 48 (2018) 311–331, https://doi.org/10.1053/j.semnuclmed.2018.02.006.

[218] P.J. Slomka, T. Pan, G. Germano, Recent advances and future Progress in PET instrumentation, Semin. Nucl. Med. 46 (2016) 5–19, https://doi.org/10.1053/j.semnuclmed.2015.09.006.

[219] S.R. Cherry, T. Jones, J.S. Karp, J. Qi, W.W. Moses, R.D. Badawi, Total-body PET: maximizing sensitivity to create new opportunities for clinical research and patient care, J. Nucl. Med. 59 (2018) 3–12, https://doi.org/10.2967/jnumed.116.184028.

[220] L. Martí-Bonmatí, R. Sopena, P. Bartumeus, P. Sopena, Multimodality imaging techniques, Contrast Media Mol. Imaging. 5 (2010) 180–189, https://doi.org/10.1002/cmmi.393.

[221] T. Beyer, L.S. Freudenberg, D.W. Townsend, J. Czernin, The future of hybrid imaging—part 1: hybrid imaging technologies and SPECT/CT, Insights Imaging. 2 (2011) 161–169, https://doi.org/10.1007/s13244-010-0063-2.

[222] T. Beyer, D.W. Townsend, J. Czernin, L.S. Freudenberg, The future of hybrid imaging—part 2: PET/CT, Insights Imaging. 2 (2011) 225–234, https://doi.org/10.1007/s13244-011-0069-4.

[223] T. Beyer, L.S. Freudenberg, J. Czernin, D.W. Townsend, The future of hybrid imaging—part 3: PET/MR, small-animal imaging and beyond, Insights Imaging. 2 (2011) 235–246, https://doi.org/10.1007/s13244-011-0085-4.

[224] H.F. Wehrl, A.W. Sauter, M.R. Divine, B.J. Pichler, Combined PET/MR: a technology becomes mature, J. Nucl. Med. 56 (2015) 165–168, https://doi.org/10.2967/jnumed.114.150318.

[225] M. Nahrendorf, E. Keliher, B. Marinelli, P. Waterman, P.F. Feruglio, L. Fexon, M. Pivovarov, F.K. Swirski, M.J. Pittet, C. Vinegoni, R. Weissleder, Hybrid PET-optical imaging using targeted probes, Proc. Natl. Acad. Sci. U. S. A. 107 (2010) 7910–7915, https://doi.org/10.1073/pnas.0915163107.

[226] M.D. Majmudar, J. Yoo, E.J. Keliher, J.J. Truelove, Y. Iwamoto, B. Sena, P. Dutta, A. Borodovsky, K. Fitzgerald, M.F. Di Carli, P. Libby, D.G. Anderson, F.K. Swirski, R. Weissleder, M. Nahrendorf, Polymeric nanoparticle PET/MR imaging allows macrophage detection in atherosclerotic plaques, Circ. Res. 112 (2013) 755–761, https://doi.org/10.1161/CIRCRESAHA.111.300576.

[227] F. Liu, H. Jang, R. Kijowski, T. Bradshaw, A.B. McMillan, Deep learning MR imaging–based attenuation correction for PET/MR imaging, Radiology. 286 (2018) 676–684, https://doi.org/10.1148/radiol.2017170700.

[228] N. Belcari, R. Boellaard, M. Morrocchi, in: D. Volterrani, P.A. Erba, I. Carrió, H.W. Strauss, G. Mariani (Eds.), PET/CT and PET/MR Tomographs: Image Acquisition and Processing BT - Nuclear Medicine Textbook: Methodology and Clinical Applications, Springer International Publishing, Cham 2019, pp. 199–217, https://doi.org/10.1007/978-3-319-95564-3_9.

[229] A. Hosny, C. Parmar, J. Quackenbush, L.H. Schwartz, H.J.W.L. Aerts, Artificial intelligence in radiology, Nat. Rev. Cancer 18 (2018) 500–510, https://doi.org/10.1038/s41568-018-0016-5.

[230] G. Wang, J.C. Ye, K. Mueller, J.A. Fessler, Image reconstruction is a new frontier of machine learning, IEEE Trans. Med. Imaging 37 (2018) 1289–1296, https://doi.org/10.1109/TMI.2018.2833635.

[231] M.N. Wernick, Y. Yang, J.G. Brankov, G. Yourganov, S.C. Strother, Machine learning in medical imaging, IEEE Signal Process. Mag. 27 (2010) 25–38, https://doi.org/10.1109/MSP.2010.936730.

[232] J. Shiraishi, Q. Li, D. Appelbaum, K. Doi, Computer-aided diagnosis and artificial intelligence in clinical imaging, Semin. Nucl. Med. 41 (2011) 449–462, https://doi.org/10.1053/j.semnuclmed.2011.06.004.

[233] G. Yamankurt, E.J. Berns, A. Xue, A. Lee, N. Bagheri, M. Mrksich, C.A. Mirkin, Exploration of the nanomedicine-design space with high-throughput screening and machine learning, Nat. Biomed. Eng. 3 (2019) 318–327, https://doi.org/10.1038/s41551-019-0351-1.

[234] Y. Liu, X. Chen, Efficient screening of spherical nucleic acids, Nat. Biomed. Eng. 3 (2019) 257–258, https://doi.org/10.1038/s41551-019-0391-6.

[235] J. Schoormans, C. Calcagno, M.R.R. Daal, R.C.I. Wüst, C. Faries, A. Maier, A.J.P. Teunissen, S. Naidu, B.L. Sanchez-Gaytan, A.J. Nederveen, Z.A. Fayad, W.J.M. Mulder, B.F. Coolen, G.J. Strijkers, An iterative sparse deconvolution method for simultaneous multicolor 19F-MRI of multiple contrast agents, Magn. Reson. Med. 83 (2019) 228–239, https://doi.org/10.1002/mrm.27926.

[236] O. Adir, M. Poley, G. Chen, S. Froim, N. Krinsky, J. Shklover, J. Shainsky-Roitman, T. Lammers, A. Schroeder, Integrating artificial intelligence and nanotechnology for precision Cancer medicine, Adv. Mater. 32 (2019) https://doi.org/10.1002/adma.201901989 1901989.

[237] X. Sun, W. Cai, X. Chen, Positron emission tomography imaging using Radiolabeled inorganic nanomaterials, Acc. Chem. Res. 48 (2015) 286–294, https://doi.org/10.1021/ar500362y.

[238] D. Chen, C.A. Dougherty, D. Yang, H. Wu, H. Hong, Radioactive Nanomaterials for Multimodality Imaging, Tomogr. (Ann Arbor, Mich.), 2, 2016 3–16, https://doi.org/10.18383/j.tom.2016.00121.

[239] A. Andreyev, A. Sitek, A. Celler, EM reconstruction of dual isotope PET using staggered injections and prompt gamma positron emitters, Med. Phys. 41 (2014) 22501, https://doi.org/10.1118/1.4861714.

[240] R.S. Miyaoka, W.C.J. Hunter, A. Andreyev, L. Pierce, T.K. Lewellen, A. Celler, P.E. Kinahan, Dual-radioisotope PET data acquisition and analysis, 2011 IEEE Nucl. Sci. Symp. Conf. Rec 2011, pp. 3780–3783, https://doi.org/10.1109/NSSMIC.2011.6153715.

[241] J.C. Knight, M.J. Mosley, V. Kersemans, G.M. Dias, P.D. Allen, S. Smart, B. Cornelissen, Dual-isotope imaging allows in vivo immunohistochemistry using radiolabelled antibodies in tumours, Nucl. Med. Biol. 70 (2019) 14–22, https://doi.org/10.1016/j.nucmedbio.2019.01.010.

[242] P. Zou, H. Chen, H.J. Paholak, D. Sun, Noninvasive fluorescence resonance energy transfer imaging of in vivo premature drug release from polymeric nanoparticles, Mol. Pharm. 10 (2013) 4185–4194, https://doi.org/10.1021/mp4002393.

[243] L. Wang, L. Yan, J. Liu, C. Chen, Y. Zhao, Quantification of nanomaterial/nanomedicine trafficking in vivo, Anal. Chem. 90 (2018) 589–614, https://doi.org/10.1021/acs.analchem.7b04765.